Chapter 4

Interaction processes for biomolecules

Various elastic and inelastic electron interaction processes are quantified in terms of cross-sections for nucleosides (Adenosine, Guanosine, Cytidine, Thymidine and Uridine), furfural, para-Benzoquinone (pBQ), pentafluoropropionitrile and heptafluorobutyronitrile for the impact energy range, IE to 5000 eV. Various correlation studies are also attempted for all these molecular systems.

4.1 Nucleosides

Nucleosides are referred to as glycosylamines, which are nucleotides lacking phosphate groups. These are the structural building blocks of nucleic acids and are necessary for all biological systems [1,2]. Tumours and viruses are treated with these nucleosides by either preventing the formation of new cancer cells or viruses through the use of nucleic acid chain terminators [3] or by selectively inhibiting enzymes required for cancer or viral replication [4]. In many fields of chemistry and biology, nucleosides and their analogues are of interest. Their structural characterisation is especially helpful in the synthesis of nucleoside analogues for the investigation of their anticoagulant effects and in the detection of the structure and sequence of changed nucleosides in ribonucleic acid (RNA) [5–7].

Numerous studies have examined the effects of electron collisions on nucleobases (DNA damage caused by electrons) [8–13], but more recent research (Deng et al. 2005) on base-sugar complex nucleosides has shown that sugar damage [14–16] predominates in nucleoside damage pathways. Moreover, Wintstead and McKoy [17–19] investigated the impact of low energy electrons on nucleosides. Thus, in the present contribution, we looked into the impact of electrons on nucleosides (Adenosine, Guanosine, Cytidine, Thymidine and Uridine).

The determination of various cross-sections for several molecular processes due to collisions between electrons and biomolecules is a vital initial step in modelling the cell damage generated by electrons (ionising radiations) directly or indirectly. Consequently, it is necessary to evaluate the cross-sections for electron interaction with biomolecules in order to comprehend and simulate the cell damage effectively [20–22].

The SCOP formalism was used in the current study to quantify different molecular elastic and inelastic processes through cross-sections for energy spectrum, from *IE* to 5000 eV. For the nucleosides under study, several cross-sections, including Q_{inel}, Q_{el}, Q_{ion}, Q_{exc}, and Q_T, have been evaluated. The entire geometrical structure of nucleosides is depicted in figure 4.1.

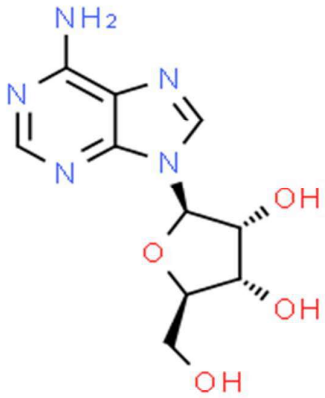

Adenosine ($C_{10}H_{13}N_5O_4$)

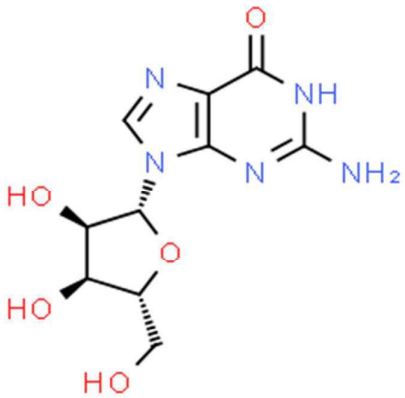

Guanosine ($C_{10}H_{13}N_5O_5$)

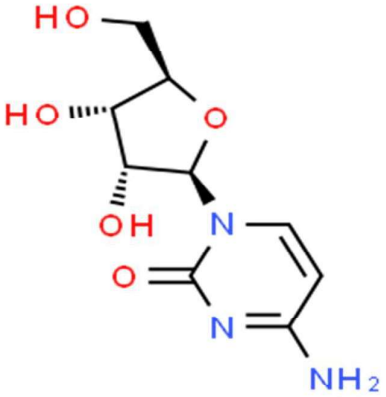

Cytidine ($C_9H_{13}N_3O_5$)

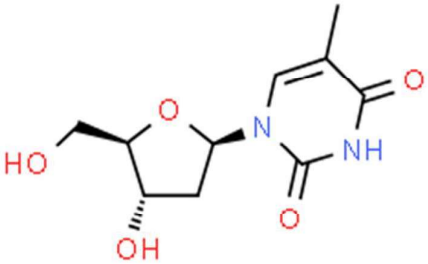

Thymidine ($C_{10}H_{14}N_2O_5$)

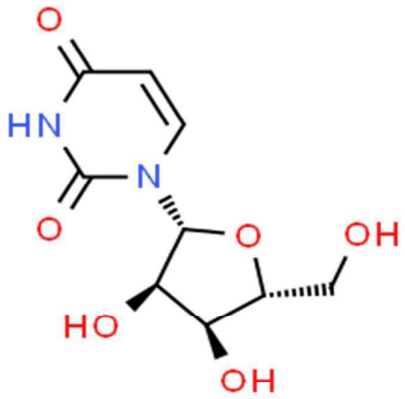

Uridine ($C_9H_{12}N_2O_6$)

Figure 4.1 Geometrical structure of nucleosides

(http://www.chemspider.com/Default.aspx)

4.1.1 Theoretical Methodology

In order to determine the cross-sections from the ionisation energy to 5000 eV, we use the SCOP approach with a multi-center group additivity method [23,24]. Studies of electron scattering can be conducted using a variety of additivity rules [25]. The requirement that the small groups of constituent atoms serve as distinct scattering centres for the small groups of big molecules supports the idea that multi-centre group formation. The group additivity approach is better suitable for large molecules like those examined here since the target system manifests as several scattering centres when the electron's wavelength decreases with the energy. So, we used this method to observe the impacts of different groups on the cross-section. Moreover, the SCOP method makes use of spherical potential, which can be explained by superimposing smaller atoms' charge density on that of bigger atoms within the groups. The multi-centre group additivity approach identifies the various scattering centres of the target molecule while also accounting for molecular geometry. The characteristics of molecules are shown in table 4.1.

Table 4.1 Molecular properties

Molecule	**IE (eV)** [26a]	**Polarisability (α) in Å^3** [27]

Adenosine	8.4	23.8
Guanosine	8.0	24.1
Cytidine	8.6	20.9
Thymidine	8.7	22.1
Uridine	9.0	20.9

4.1.2 Results and Discussion

As a function of incident energy from the molecular ionisation threshold to 5000 eV, the various cross-sections, (viz., Q_{inel}, Q_{el}, Q_T, Q_{ion} and ΣQ_{exc}) for all the present investigated biomolecules are computed in the present study [26b] and shown in this section.

A. Inelastic effects

Figures 4.2 to 4.6 illustrate the Q_{inel}, which covers the ionisation and excitation effects for electron interaction with nucleosides (adenosine, cytidine, guanosine, uridine, and thymidine).

The uppermost curves in each of these figures represent Q_{inel}, whereas the lowermost curves represent total electronic excitation cross-sections, $\sum Q_{exc}$. We emphasise that present study is the first effort to describe these cross-sections of all these biomolecules under study.

Total ionisation cross-sections derived from Q_{ion} data is represented by the centre curves. Until today, no theoretical or experimental research on the electron interaction cross-sections of these nucleosides have been conducted, except by Mozejko [28]. Furthermore, they only estimated the Q_{ion} for four of the nucleosides, namely adenosine, guanosine, cytidine, and uridine, using the BEB formalism from the ionisation threshold to 200 eV.

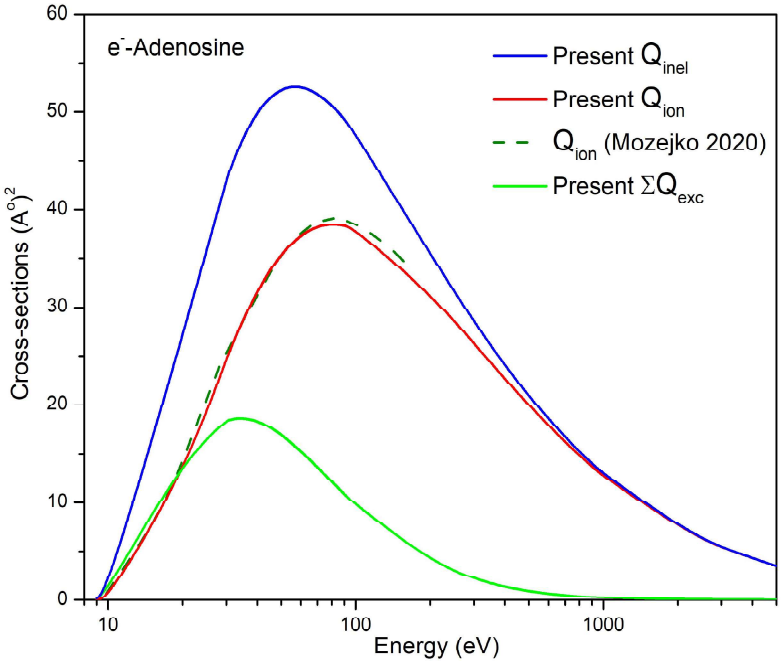

Figure 4.2 Q_{inel}, Q_{ion} and $\sum Q_{exc}$ for Adenosine

Blue: Present Q_{inel}; Red: Present Q_{ion}; Olive green dash: Mozejko Q_{ion} [28]*; Green: Present $\sum Q_{exc}$*

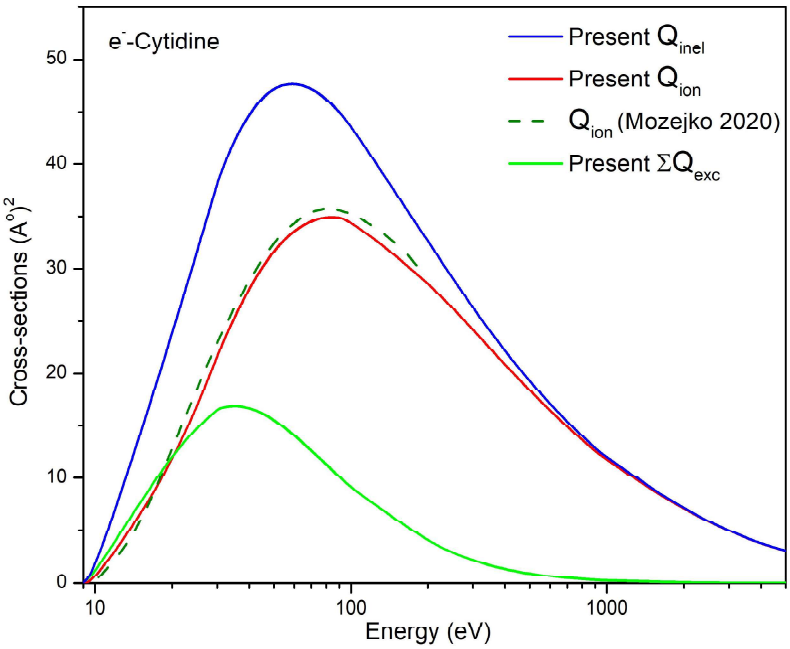

Figure 4.3 Q_{inel}, Q_{ion} and $\sum Q_{exc}$ for Cytidine

Blue: Present Q_{inel}; Red: Present Q_{ion}; Olive green dash: Mozejko Q_{ion} [28]*; Green: Present $\sum Q_{exc}$*

Figures 4.2 to 4.5 compare the present Q_{ion} to the Q_{ion} of [28] estimated using BEB. The present curves for adenosine and cytidine (figures 4.2 and 4.3) demonstrate excellent agreement with the Binary Encounter Bethe (BEB) data [28], however the current Q_{ion} values for guanosine and uridine (figures 4.4 and 4.5) are marginally higher within the specified uncertainty of ±15% of BEB data [28]. The cross sections are very much dependent on the ionisation energy employed. The BEB data [28] are up to 200 eV, and we notice that the present Q_{ion} and that of [28] tend to merge beyond the peak region.

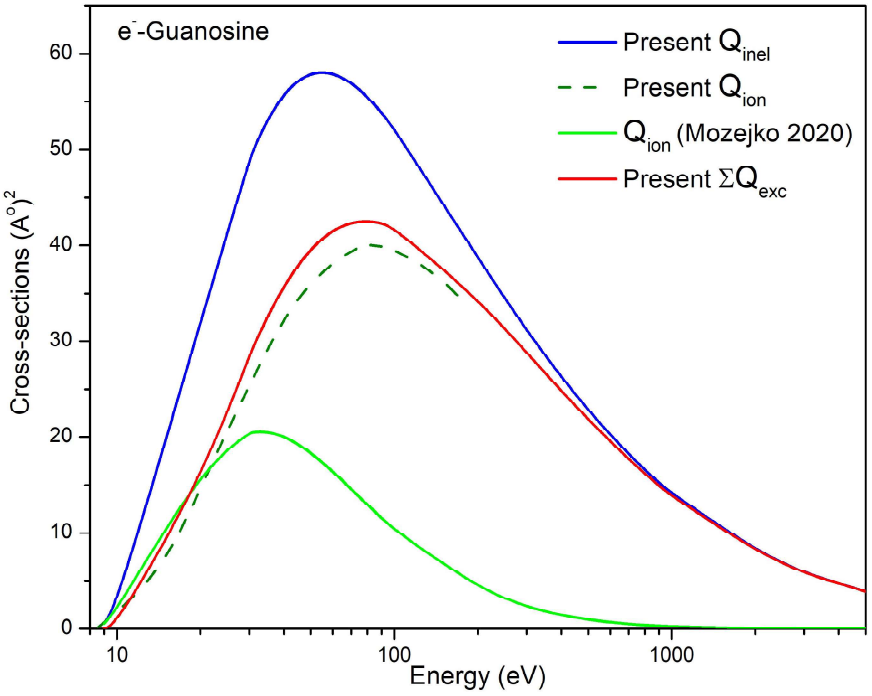

Figure 4.4 Q_{inel}, Q_{ion} and $\sum Q_{exc}$ for Guanosine

Blue: Present Q_{inel}; Red: Present Q_{ion}; olive green dash: Mozejko Q_{ion} [28]*; Green: Present $\sum Q_{exc}$*

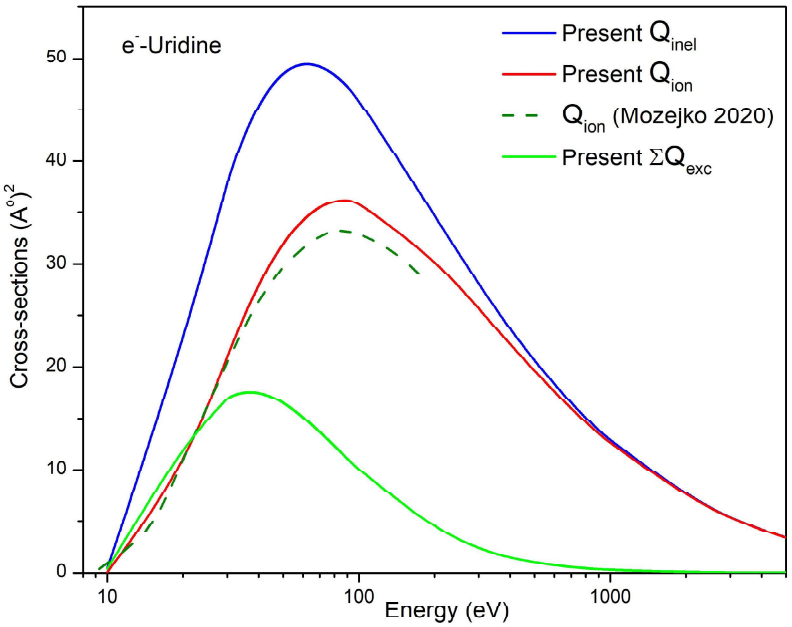

Figure 4.5 Q_{inel}, Q_{ion} and $\sum Q_{exc}$ for Uridine

Blue: Present Q_{inel}; Red: Present Q_{ion}; Olive green dash: Mozejko Q_{ion} [28]*; Green: Present $\sum Q_{exc}$*

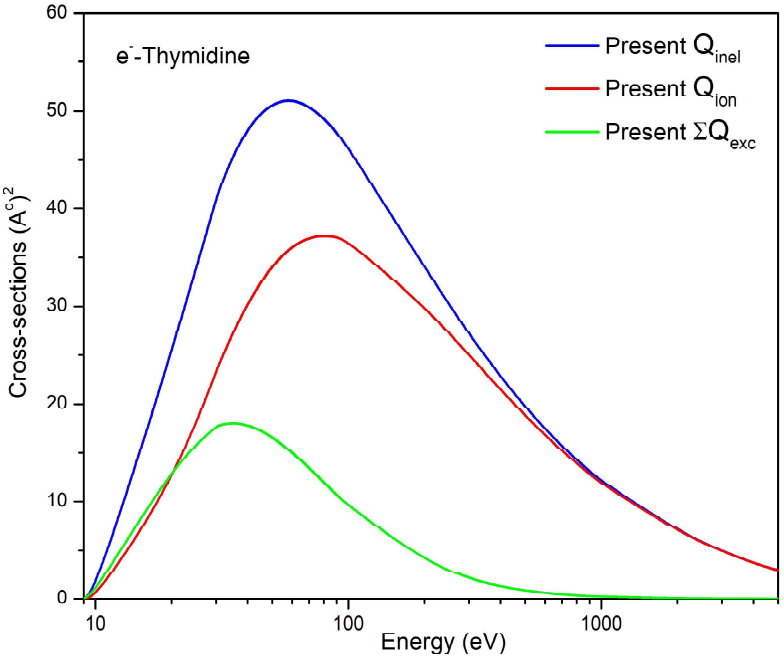

Figure 4.6 Q_{inel}, Q_{ion} and $\sum Q_{exc}$ for Thymidine

Blue: Present Q_{inel}; Red: Present Q_{ion}; Olive green dash: Mozejko Q_{ion} [28]*; Green: Present $\sum Q_{exc}$*

No cross-sections data for thymidine are available for the comparison (figure 4.6). Present study is the first report on electron interaction cross-sections results for thymidine. As energetic electrons transfer their kinetic energy to molecular systems, the inelastic cross sections increase with the incident energies. At higher energies, however, these probabilities decrease as $\frac{1}{E_i}$ beyond the peak energy. The peak value is determined by electron energy and interaction time between incident electrons and the molecular target.

B. Elastic effects

The Q_T and the elastic cross-sections, Q_{el} are depicted in figures 4.7 and 4.8, respectively, where N denotes the molecule size in terms of the electron number. The Q_T includes every elastic and inelastic event driven by an incoming electron.

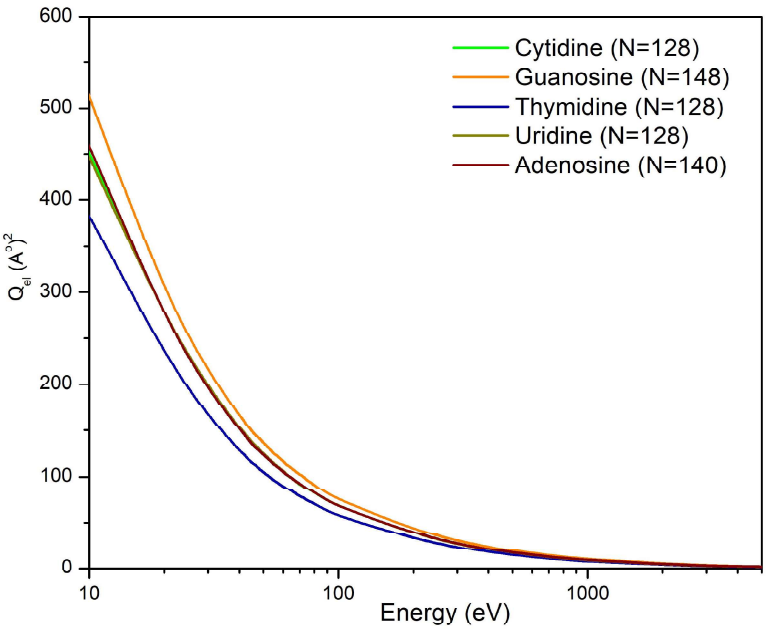

Figure 4.7 Q_{el} for all Nucleosides

Green Line: Cytidine; Orange line: Guanosine; Blue line: Thymidine; Dark yellow line: Uridine; Wine line: Adenosine

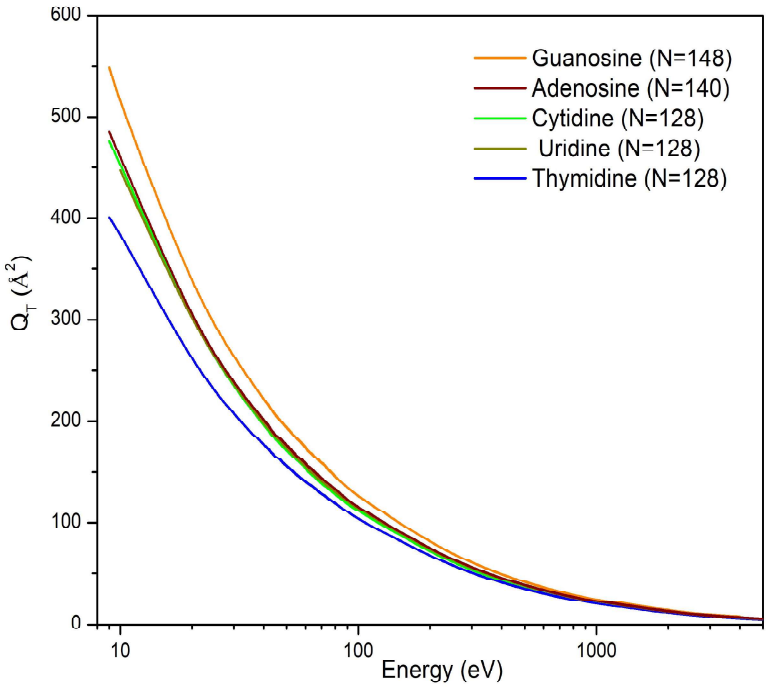

Figure 4.8 Q_T for all Nucleosides

Red line: Adenosine; Blue line: Guanosine; Black line: Cytidine; Green line: Thymidine; Dark yellow line: Uridine

The probability that all electron-induced molecular events will take place, are represented by Q_T, which is employed in several modelling methodologies [29,30]. As can be seen, Q_T drops as $\frac{lnE_i}{E_i}$ in the high energy regime and exhibits the trend of Born-Bethe [31]. Figures 4.7 and 4.8 further show the size dependence of Q_{el} and Q_T.

Figure 4.9 shows a relative estimation of various quantified chemical processes for e^- - Uridine collision at E_p = 62 eV. While Q_T is the upper bound for electron-induced events, Q_{el} and Q_{inel} make up 68% and 32% of Q_T, respectively. As expected, $\sum Q_{exc}$ contributes 30% while Q_{ion} makes up 70% of Q_{inel}.

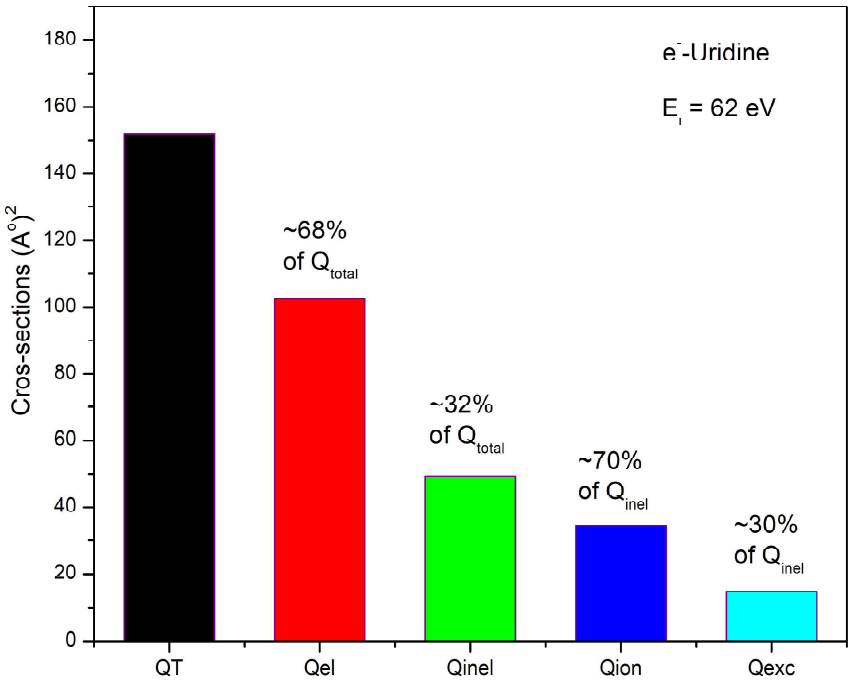

Figure 4.9 Relative estimation of various quantified molecular processes

We were able to provide several forms of electrons induced scattering cross-sections data using our theoretical framework that was explained earlier. However, the current theory requires approximation since a spherical potential must be built and the charge density must be modelled using the group additivity rule. The final data generated by these approximations contains an uncertainty of 10% to 15%, which is comparable to the majority of experimental data. As a result, the information provided here is trustworthy enough to be used in applicable domains like radiology and the biological field.

4.2 Furfural ($C_5H_4O_2$) and para-Benzoquinone ($C_6H_4O_2$)

Over the past few decades, there has been a growing interest in the development of new or improved technologies (in terms of sustainability and low cost), in particular for the conversion of lignocellulosic biomass into several biomaterials including biofuels [32]. This interest was sparked by a situation in which the growing global demand for energy [33] must be satisfied while at the same time voicing concerns about climate change. When it comes to the challenges that need to be overcome, "biomass recalcitrance" is the one that has the most significant impact on the high cost of converting lignocellulose into biomaterials that have a

high value-added. According to theoretical and experimental research aimed at finding a solution to this question [34–36], atmospheric pressure plasmas that generate radicals and free electrons can facilitate the breakdown of biomass by producing dissociations, excitations, and other fragmentation processes. Consequently, we have investigated the effects of electron collisions on Furfural, a byproduct of certain lignocellulose species that could one day serve as a replacement for petroleum-based compounds [37].

2-furaldehyde, also known as furfural ($C_5H_4O_2$), plays an important part in green chemistry [38]. It additionally finds applications in the production of petroleum, agrochemicals, medicines, and polymers. In addition to this, it has been acknowledged as an essential chemical building block [37,39] for the commercialization of biorefineries. The process of converting biomass into biofuel begins with irradiating it with electron beams or subjecting it to atmospheric pressure plasma [34,40]. This first step improves the conversion yield significantly. This, along with other modelling plasma applications [41], points to the necessity for accurate and exhaustive electron scattering data for furfural [42].
The chemical structure of $C_5H_4O_2$ molecule is given in figure 4.10.

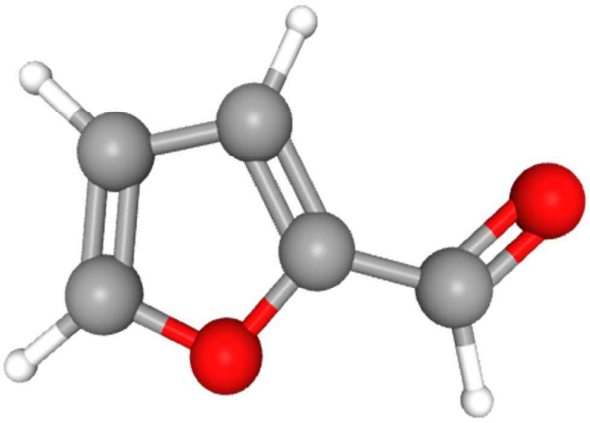

Figure 4.10 Chemical structure of Furfural
(https://pubchem.ncbi.nlm.nih.gov)

As global energy consumption continues to rise, the challenges associated with gathering and storing energy in a manner that is environmentally friendly are becoming an increasingly pressing concern. Learning from and modelling ourselves after nature could pave the way for innovations that could help solve these problems. Oxygenic photosynthesis is the primary means by which energy is converted into usable form on Earth. During this process, water

and carbon dioxide are converted into oxygen and carbohydrates [43]. Therefore, increasing our understanding of these photosynthetic processes may be able to stimulate breakthroughs in photocatalysis and photovoltaics [44], as well as the creation of hybrid photo-bio electrochemical technologies [45]. Quinones are an essential molecular component in the sequence of photosynthesis that involves cellular respiration and the transfer of electrons because they are capable of carrying out reversible reduction processes. Accordingly, they are proving to be a long-term, cost-effective material in energy-harvesting and storage systems like artificial photosynthetic platforms, rechargeable batteries, pseudo-capacitors, phototransistors, plasmonic light harvesting platforms, and dye-sensitized solar cells. A deeper knowledge of the unique characteristics of quinone and its derivatives can aid in the design of bio-inspired energy conversion and harvesting systems. In this regard, para-benzoquinone (pBQ), which is the simplest quinone, has acted as a prototype structure in a range of study attempting to understand the electrochemical and photon induced behaviour of quinones in general.

Since this molecule has garnered a lot of attention recently, we have zeroed in on to this molecule and investigated the processes involved in its electron interactions from the molecular ionisation threshold up to 5 keV in the present work. Figure 4.13 displays the chemical structure of this pBQ ($C_6H_4O_2$) molecule.

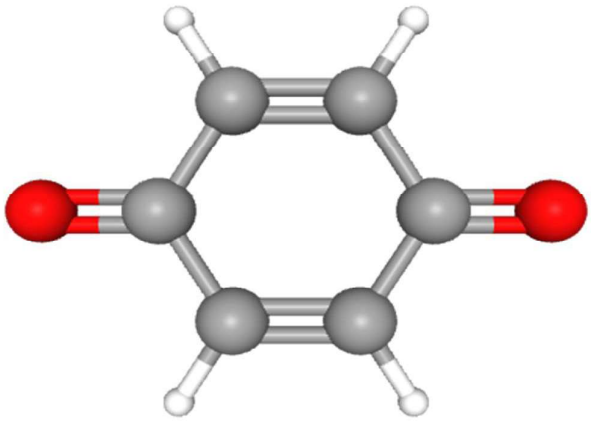

Figure 4.11 Chemical structure of para-Benzoquinone

(https://pubchem.ncbi.nlm.nih.gov)

4.2.1 Literature survey and Target properties

Table 4.2 Literature survey for Furfural and para-Benzoquinone

Molecules	Quantity	Methods	E_i (eV)	References
Furfural ($C_5H_4O_2$)	Q_{ion}	Binary-Encounter-Bethe (BEB) [Th.]	1-1000	Jones *et al* (2016) [42]
	Q_{inel}, Q_{el}, Q_T	IAM-SCAR+I [Th.]		
	Q_{exc}	Energy loss spectra [Ex.]	20,30,40,50 ,250	
	Q_{exc}	Discrete inelastic [Th.]	1-1000	
	Q_T	Double electrostatic analyzer gas cell electron transmission cell [Ex.]	10-1000	Traore Dubuis *et al* (2017) [46]
	Q_T	IAM-SCAR+I & Semi-empirical model [Th.]	500-10000	
	Q_T	Electron Transmission Experiment [Ex.]	7, 10, 20	Lozano *et al* (2017) [47]
pBQ ($C_6H_4O_2$)	Q_T	Transmission-beam attenuation measurements [Ex. ±5%]	1-200	Lozano *et al* (2018) [48]
	Q_{inel}, Q_{ion}, Q_{el}, Q_T, Q_{exc}	IAM-SCAR+I [Th.]		
	Q_{el},	SMCPP [Th.]	1-50	
	Q_{exc}	Energy loss spectra [Ex.]	20,30,40	Jones *et al* - (2018) [49]
	Q_{inel}, Q_{el}, Q_T, Q_{exc}	IAM-SCAR+I [Th.]	10-1000	
	Q_{ion}	BEB [Th.]	10-1000	
	Q_{inel}, Q_{el}, Q_T, Q_{ex}	SMCPP [Th.]	16-50	

Table 4.3 Target properties of Furfural and para-Benzoquinone (http://www.chemspider.com)

Target	IE (eV)	Polarizability (α) in $A°^3$

Furfural	9.21	10.0
para-Benzoquinone	10.01	10.8

4.2.2 Results and Discussion

The present work involves the determination of electron interaction cross sections with furfural ($C_5H_4O_2$) and para-Benzoquinone ($C_6H_4O_2$) with impact energies ranging from *IE* to 5000 eV (Q_{inel}, Q_T, Q_{el}, Q_{ion}, and ΣQ_{exc}). To aid our explanation, the theoretical results are shown in figures 4.12 and 4.15 alongside the existing data.

A. Inelastic effects

Present inelastic, ionisation, and electronic excitation cross sections for furfural are plotted in figure 4.12. The topmost curve shows Q_{inel}, which is compared with the only available data of Jones *et.al.* [42]. They used Independent Atom Model with Screening Corrected Additivity Rule including Interference (IAM-SCAR+I) method. Throughout the energy range present Q_{inel} shows good accord with that of Jones *et.al.* [42] except at the peak region, where present Q_{inel} slightly overestimates the IAM-SCAR+I result.

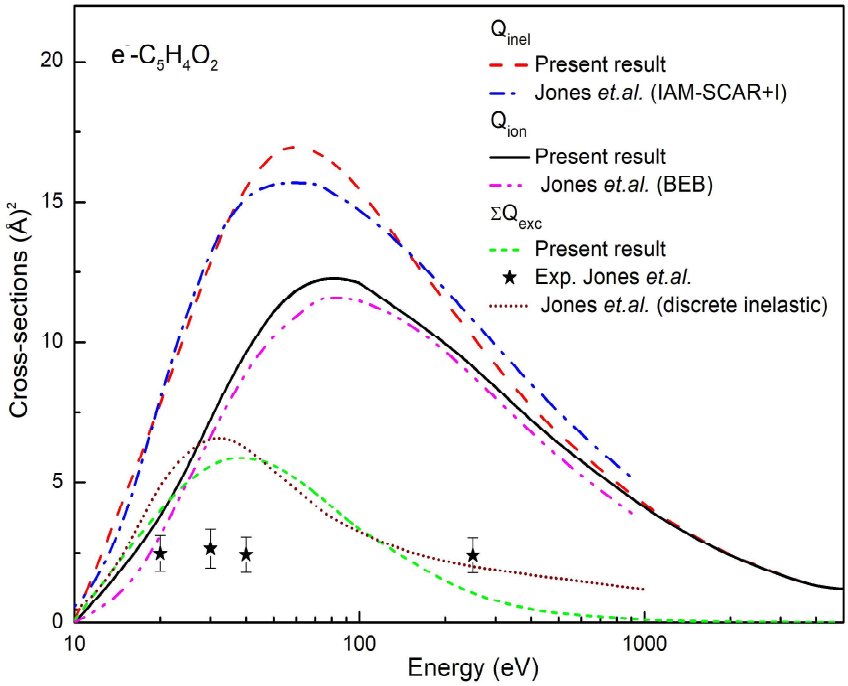

Figure 4.12 Q_{inel}, Q_{ion}, and $\sum Q_{exc}$ for e^--$C_5H_4O_2$ (furfural)

Red dash: Present Q_{inel}; Blue dash dot: Jones et.al. [42] *Q_{inel} using IAM-SCAR+I method; Black solid: Present Q_{ion}; Magenta dash dot dot: Jones et.al.* [42] *Q_{ion} using BEB method, Green short dash: Present ΣQ_{exc}; Black filled stars: Jones et.al.* [42] *experimental Q_{exc}, Wine short dot: Jones et.al.* [42]

The present Q_{ion} is shown through the middle solid line in figure 4.12. Only Jones *et.al.* [42] has reported the Q_{ion} results using BEB theory and present data are seen to be in excellent accord with them within the mentioned 15% uncertainty of BEB [50]. The lowest curve represents the calculated $\sum Q_{exc}$. It is compared with both theoretical and experimental excitation cross sections of Jones *et.al.* [42]. Their calculated data overestimates the present $\sum Q_{exc}$. The experimental electronic excitation cross-sections for the bands I-VI separately and their sum (summed Q_{exc}(band I+II+III+IV+V+VI)), both have been reported by Jones *et.al*. [42] for the energy spectrum, 20-250 eV with the mentioned uncertainty 18% to 69%. This summed Q_{exc} is compared with the present $\sum Q_{exc}$ and seen to be of lower values than present ones (includes all the allowed electronic excitations), as expected. Jones *et.al.* [42] computed the discrete inelastic data by excluding the Q_{ion} from the total Q_{inel}. This discrete inelastic data has been also compared with the Q_{exc} and can be seen in good agreement with the present ones.

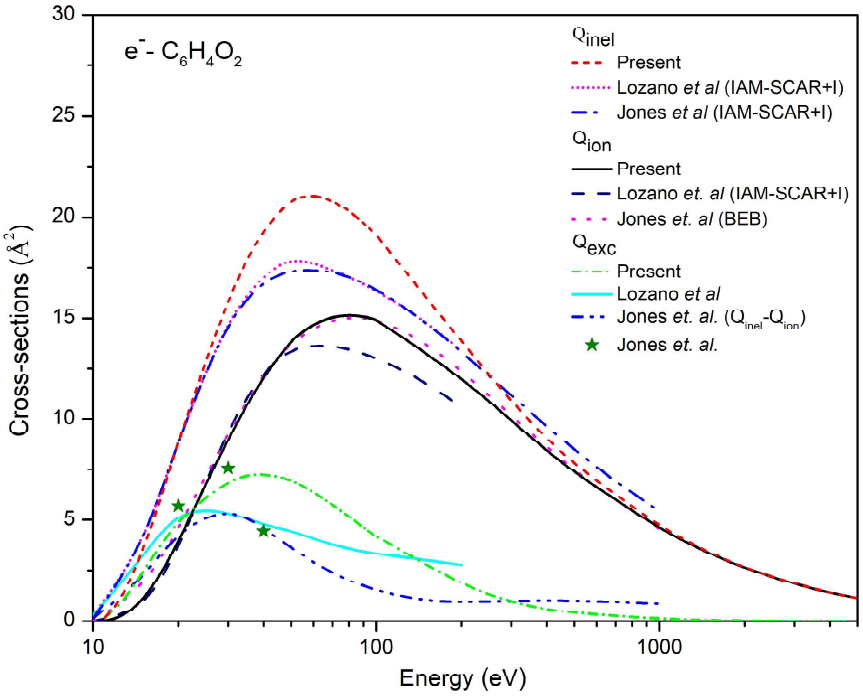

Figure 4.13 Q_{inel}, Q_{ion}, and $\sum Q_{exc}$ for e^- - $C_6H_4O_2$ (para-Benzoquinone)

Red short dash: Present Q_{inel}, Magenta short dots: Lozano et.al. [48] *Q_{inel} using IAM-SCAR+I method; Violet dash dot: Jones et.al.* [49] *Q_{inel} using IAM-SCAR+I method; Black solid: Present Q_{ion}; Navy blue dash: Lozano et.al.* [48] *Q_{ion} IAM-SCAR+I method; Dark yellow dot: Jones et.al.* [49] *Q_{ion} using BEB formalism; Green dash dot: Present ΣQ_{exc}, Orange dash dot dot: Jones et.al. (Q_{inel}-Q_{ion})* [49]*; Olive green filled stars: Jones et.al.* [49]

The topmost curve in figure 4.13 displays the Q_{inel} for para-Benzoquinone ($C_6H_4O_2$) with data of Lozano *et.al.* [48] and Jones *et.al.* [49]. Both the authors [48,49] have employed IAM-SCAR+I approach. Except at the peak region, present results show good agreement with the existing ones [48,49]. Present ionization cross-sections compared with available theoretical data obtained from IAM-SCAR+I [48] and BEB [49] approaches are shown in figure 4.13. From the figure it can be observed that the present Q_{ion} data matches excellently well with the result of Jones *et.al.* [49]. However, the data of Lozano *et.al.* [48] which are up to 200 eV, underestimates both, present and Jones *et.al.* [49] results. $\sum Q_{exc}$ computed through present methodology along with the available comparisons is also presented in this figure 4.13. The theoretical excitation cross sections calculated using IAM-SCAR+I method [48], [49] are

observed to be in good agreement with the present results below 25 eV. Jones *et.al.* [49] has also measured the Q_{exc} for each bands 0 to V from 20-40 eV energies. Their reported sum values (Q_{exc}(0+I+II+III+IV+V)) have been compared here with the present $\sum Q_{exc}$ and good agreement can be observed for 20 and 30 eV.

B. Elastic effects

In figure 4.14 present Q_{el} and Q_T are illustrated for the electron collision with Furfural molecule. The sole data of Jones *et.al.* [42] available for Q_{el}, which has been compared with the present one. At low energies a deviation between both of them can be observed, which is due to the fact that the present Q_{el} has been calculated in the presence of inelastic channels while Jones *et. al.* [42] has computed the pure Q_{el}. The uncertainty in their calculation of elastic cross sections is up to 43% at 1000 eV due to interference term added [42]. The Q_T calculated using present SCOP method is also plotted in figure 4.14 with the existing data of Jones *et.al.* [42], Lozano *et.al.* [47] and Traoré Dubuis *et.al.* [46]. The discrepancies between the present data and all the existing ones can be observed from the figure 4.14. However, the present results of Q_T show the same trend as that of Jones *et.al.* [42]. While present calculation does not involve the non-spherical effects, Jones *et.al.* [42] have considered the involvement of rotational excitations into Q_T. This may be the reason for the discrepancy between the present data and results of Jones *et.al.* [42]. The experimental Q_T data of Traoré Dubuis *et.al.* [46] also seen in reasonable agreement with the present ones within the mentioned uncertainty of 4% - 22% above 50 eV [46]. Traoré Dubuis *et.al.* [46] have also calculated the Q_T for energy above 500 eV, using a semi-empirical model (SEM) proposed by Garcŕa and Manero [51], for molecules having up to 22 electrons. They [46] claimed that their SEM model never been validate for ring molecular targets having higher atomic numbers. The present results for Q_{el} and Q_T estimated using 2p-SEM formalism is also plotted in figure 4.14. These 2p-SEM results are seen to be underestimated at lower energy side while following the similar trend as others.

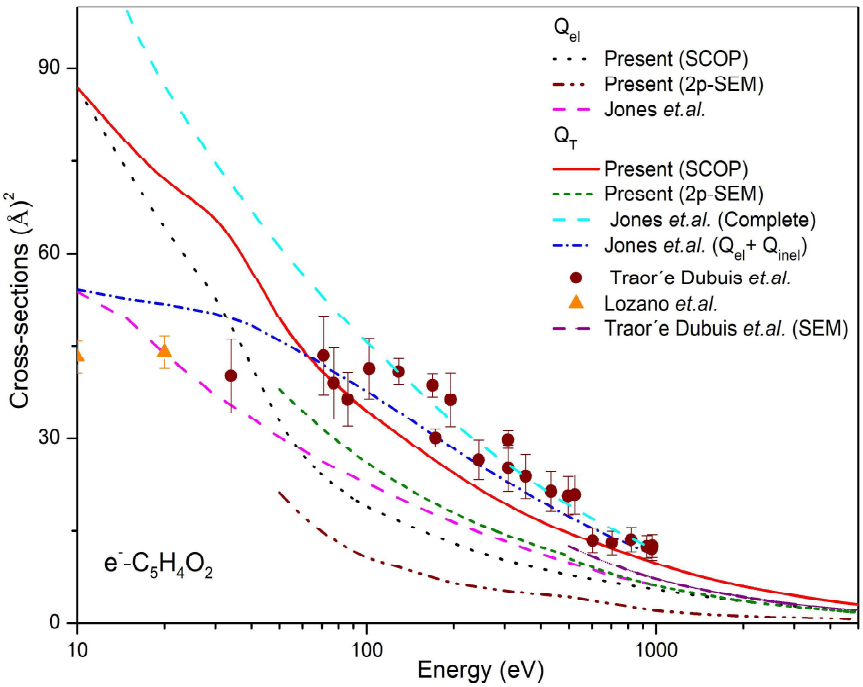

Figure 4.14 Q_{el} and Q_T for e^--$C_5H_4O_2$ (furfural)

Black dot: Present Q_{el} (SCOP), Wine dash dot dot: Present Q_{el} (2p-SEM), Magenta dash: Jones et.al. [42] *Q_{el}; Red solid: Present Q_T (SCOP), Olive short dash: Present Q_T (2p-SEM); Cyan dash: Jones et.al.* [42] *Q_T (complete); Blue short dash dot: Jones et.al.* [42] *(Q_{el} + Q_{inel}); Filled circles: Traoŕe Dubuis et.al.* [46] *Q_T; Filled triangles: Lozano et.al.* [47] *Q_T; Purple dash: Traoŕe Dubuis et.al.* [46] *Q_T (SEM)*

In figure 4.15 presents Q_{el} for electron collision with para-Benzoquinone ($C_6H_4O_2$) along with the available results, computed through IAM-SCAR+I [48,49] and SMCPP [48,49], approach have been plotted. Up to 30 eV present data overestimates with the existing theoretical results [48,49]. Beyond 30 eV present cross sections show excellent matching with the data of Lozano *et.al.* [48] and Jones *et.al.* [49], obtained through SMCPP approach. However, the present Q_{el} underestimates the results from IAM-SCAR+I approach [48]. The present Q_{el} calculated by 2p-SEM result show excellent matching with the SCOP data.

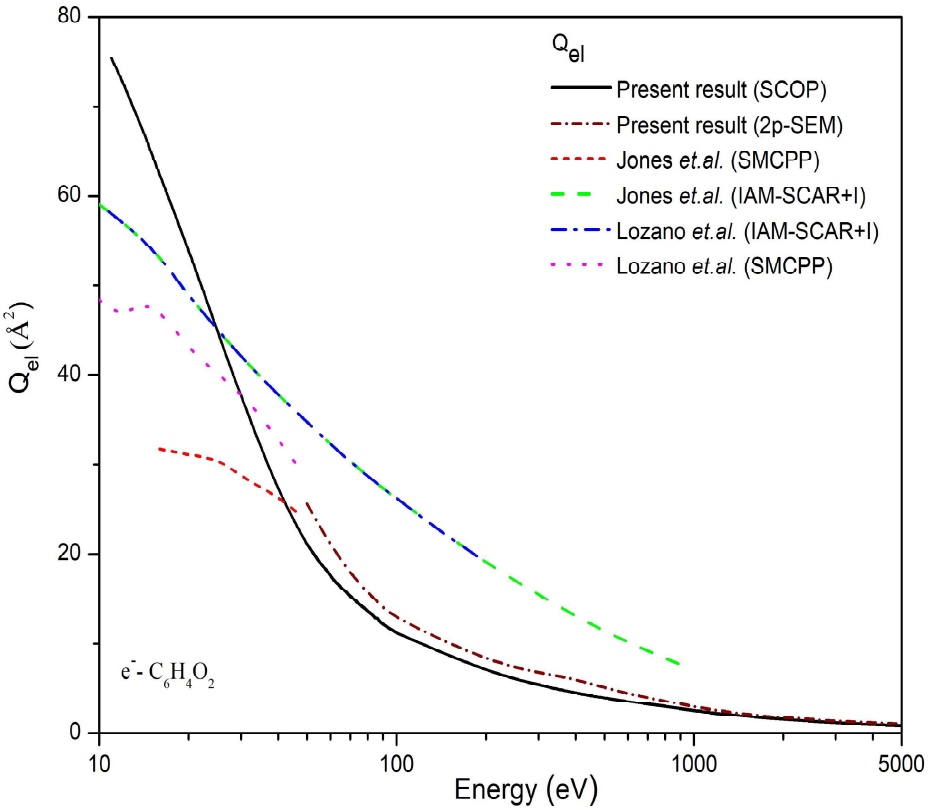

Figure 4.15 Q_{el} for e^- - $C_6H_4O_2$ (para-Benzoquinone)

Black solid: Present Q_{el} (SCOP); Wine dash dot: Present Q_{el} (2p-SEM); Magenta dot: Lozano et.al. [48] *Q_{el} using SMCPP method; Blue dash dot: Lozano et.al.* [48] *Q_{el} using IAM-SCAR+I; Green dash: Jones et.al.* [49] *Q_{el} using IAM-SCAR+I; Red short dash: Jones et.al.* [49] *Q_{el} using SMCPP method*

The present total cross sections (Q_T) are the summation of Q_{el} and Q_{inel}. In figure 4.16 present Q_T data for pBQ ($C_6H_4O_2$) has been plotted. Starting from the ionisation threshold of the molecule to 30 eV our data overestimates the theoretical results computed through IAM-SCAR+I [48], but show excellent matching with experimental [48] result within the uncertainty limit of ±5%. Present 2p-SEM result show excellent matching with the current SCOP result. Present data includes SCOP and 2p-SEM results, which show similar trend with other available results.

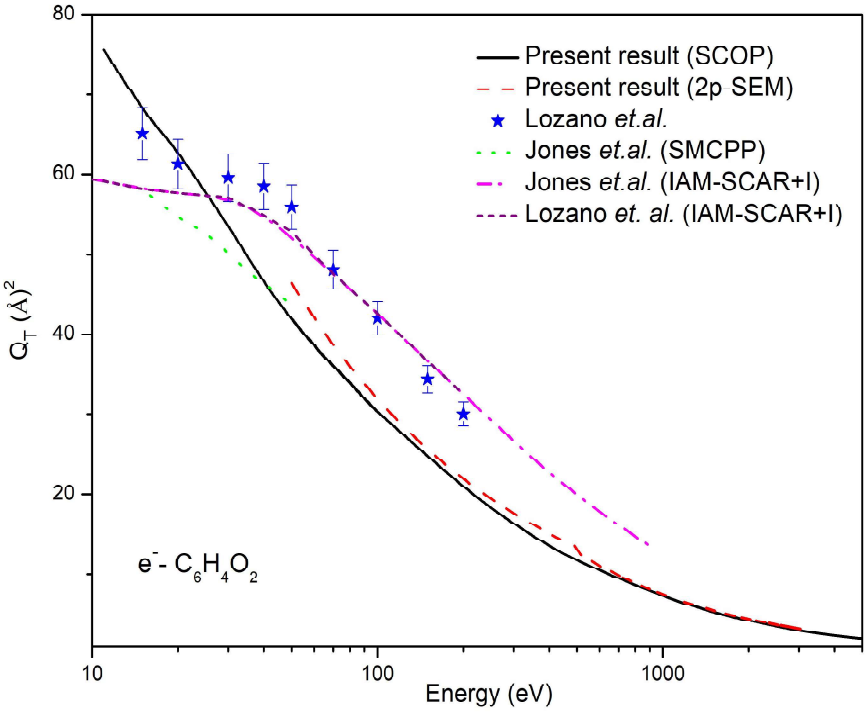

Figure 4.16 Q_T for e^- - $C_6H_4O_2$ (para-Benzoquinone)

Black solid: Present Q_T (SCOP); Red dash: Present Q_T (2p-SEM); Blue filled stars: Lozano et.al. [48] *Q_T; Green dots: Jones et.al.* [49] *Q_T using SMCPP method; Magenta dash dot: Jones et.al.* [49] *Q_T using IAM-SCAR+I approach, Purple short dash: Lozano et.al.* [48] *Q_T using IAM-SCAR+I approach*

4.3 Fluoronitriles (C_3F_5N and C_4F_7N)

The insulating gas sulphur hexafluoride (SF_6) is frequently used in high-voltage devices [52]. Numerous physical and chemical properties, such as non-toxicity, a low boiling point, and excellent insulating performance, support this choice. Due to its low land demand, low electromagnetic radiation and great dependability, SF_6-insulated equipment is widely used in high and ultra-high electrical voltage systems. However, there would be a significant financial loss if the insulation on the equipment failed. Moreover, sulphur hexafluoride degrades in the atmosphere quite slowly and has a very high global warming potential (GWP), that is 22,800 times greater than carbon dioxide. Therefore, one of the most ubiquitous and crucial concerns in the field of high-voltage mechatronics research is finding a

gas to replace SF_6. Fluoronitrile (C_4F_7N, C_3F_5N) gases have been extensively studied recently [53,54] as prospective SF_6 alternatives.

The GWP and dielectric strength of all of these three materials have been compared and listed in Table 4.4. Both fluoronitrile gases possess low GWP [55] and high dielectric strength [56] compared to SF_6.

Table 4.4 Comparison of the GWP and dielectric strength of SF_6, C_3F_5N and C_4F_7N

Molecule	ε (rel. SF_6)	GWP
C_3F_5N	2	-
C_4F_7N	2.2	2100
SF_6	1	23900

Numerous investigations on the gases C_4F_7N and C_3F_5N have been carried out on their insulating properties under various environmental conditions. Studies on microscopic elements like the ionisation cross sections upon electron impacts are, however, scarce. The Q_{ion} for electron impacts are critical variable for understanding the mechanics of electron avalanches and gas breakdown. Discharge reaction rates and gas electron transport coefficients can be calculated using Boltzmann's calculations [57] or Monte-Carlo calculations, both of which need Q_{ion} as an input criterion. Although Q_{ion} can be measured experimentally, it is not feasible to test the Q_{ion} of all potential alternative gases due to the time-consuming measuring technique, reactive, and occasionally hazardous nature of the molecules. Thus, theoretical methods develop into potent tools for obtaining Q_{ion}, which might be used as a standard for the investigation of the insulating properties of gaseous substances. The Binary-Encounter Bethe (BEB) technique [58], the Deutsch-Mark (DM) method [59], and the CSP-ic method [60] are the most well-known theoretical approaches.

For the BEB method, there are only three parameters required for the targeted molecule's initial configuration: kinetic energy, the number of occupied orbitals of an electron and orbital binding energy [58]. All of them can be readily derived from quantum chemistry calculations. Contrarily, the DM technique is a semi-empirical method that necessitates the fitting of weighting factors to experimental ionisation cross sections, notably for molecules containing a fluorine atom [59]. This is because the ionisation of these compounds using the DM method will be significantly higher than what has been observed in the studies [59].

Using a CSP-ic method, we have computed Q_{ion} for C_3F_5N and C_4F_7N. It is essential to build a complete set of electron cross sections to forecast the performance of the fluoronitriles in industrial gas discharges, plasma reactors, GIS and GIL.

4.3.1 Literature survey and Target properties

Only a few studies (table 4.5) on electron interactions with fluoronitriles have been conducted. Further, the data of Q_{el}, and Q_T have not been yet reported. In the present investigation, Q_{el} and Q_T for the mentioned fluoronitriles were calculated for the first time.

Table 4.5 Literature survey on electron impact study of fluoronitriles

Molecules	Quantity	Impact Energy (E_i) (eV)	References
C_3F_5N	Q_{ion}	IE-1000	Wang *et.al.* [61]
C_4F_7N	Q_{ion}	IE-1000	Wang *et.al.* [61]
	Q_{ion}	IE-2000	Xiong *et.al.* [59]
	Q_{ion}	IE-100	Rankovic *et.al.* [62]
	Q_{inel}, Q_{ion}, $\sum Q_{exc}$	IE-5000	Sinha *et.al.* [63]

Schematics of the fluoronitriles considered in this work are shown in figure 4.17.

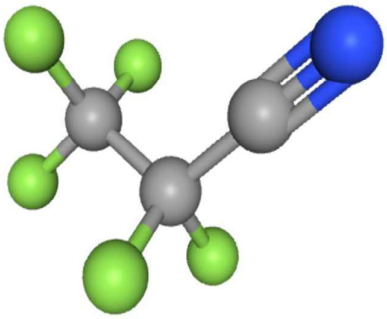

C_3F_5N (Pentafluoropropionitrile)

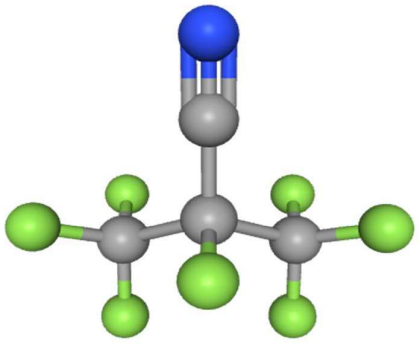

C_4F_7N (Heptafluorobutyronitrile)

Figure 4.17 Diagrammatic representations of fluoronitrile molecules

(*https://pubchem.ncbi.nlm.nih.gov*)

4.3.2 Results and Discussion

For both fluoronitriles, viz., C_3F_5N and C_4F_7N, the complete set for the electron impact cross-sections have been reported []. Various correlation studies for Q_{ion} and polarisability and dielectric constant have been also conducted.

A. Inelastic effects

Figure 4.18 displays the various inelastic cross-sections, (Q_{inel}, $Q_{ion,}$ and ΣQ_{exc}) data for C_3F_5N molecule. Wang *et.al.* [61] reported the Q_{ion} values for C_3F_5N molecule by employing the BEB method. The current Q_{ion} results for C_3F_5N matches well with those of Wang *et.al.* [61] across the whole energy range of BEB data, as can be seen in figure 4.18. At the peak region the present Qion results show high values than those of BEB results within the reported uncertainty of BEB method, which ±10% [64,65]. The present results of total Q_{inel} have been represented by the uppermost curve and present summed electronic excitation cross-sections ΣQ_{exc} is represented through the lowermost curve. Present study is the first report on these Q_{inel} and ΣQ_{exc} data for C_3F_5N molecule.

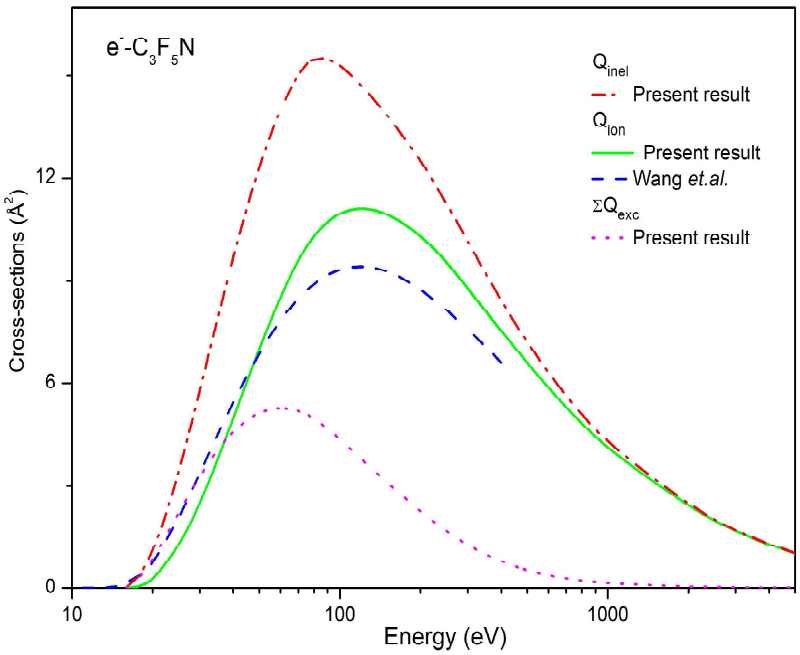

Figure 4.18 Inelastic processes for C_3F_5N

Red dash dot: Present Q_{inel}; Green solid: Present Q_{ion}; Blue dash: Wang et.al. Q_{ion} [61] *(BEB); Magenta dot: Present $\sum Q_{exc}$*

In the figure 4.19, the inelastic, ionisation and excitations cross-sections for C_4F_7N have been plotted as a function of impact energy. Present Q_{ion} data can be seen in excellent accord with those of existing ones [59] for energies from threshold to 40 eV, except Sinha *et.al.* [63]. The discrepancy between the Q_{ion} of Sinha et.al. and existing ones can be observed. This difference may be due to fact that Q_{ion} of Sinha *et.al.* [63] includes the nuclear charge effects of the molecule. At the peak region of Q_{ion}, present results show good matching with the Q_{ion} data obtained by using modified DM formalism [59]. Above the peak of Q_{ion}, the data obtained from BEB and DM calculations are seen to be of lower values than the existing ones while showing reasonable agreement up to the summit of Q_{ion}. Further, excellent accord between the present Q_{ion} and the experimental Q_{ion} of Rankovic *et.al.* [62] is observed at low energy side.

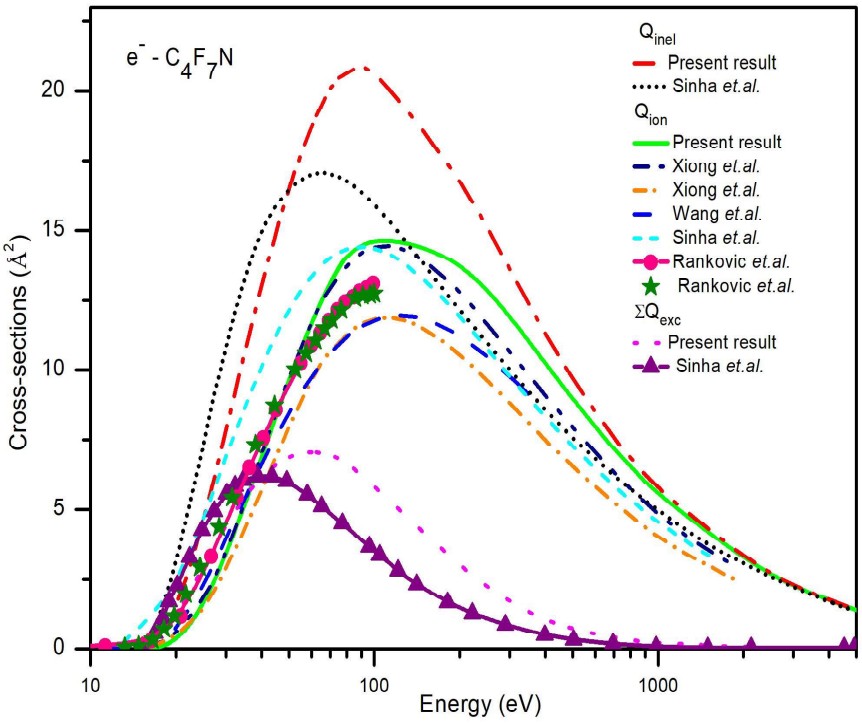

Figure 4.19 Inelastic processes for C_4F_7N

Red dash dot: Present Q_{inel}; Black short dot: Sinha et.al. Q_{inel} [63]*; Green solid: Present Q_{ion}; Blue dash: Wang et.al.* [61] *Q_{ion}; dash dot dot: Xiong et.al.* [59] *Q_{ion}; Short dashed dot: Xiong et.al.* [59] *Q_{ion}; Short Dashed: Sinha et.al.* [63] *Q_{ion}; -●- Rankovic et.al.* [62] *Q_{ion}; -■- Rankovic et. al.* [62] *Q_{ion}; Dotted: Present $\sum Q_{exc}$; -◀- line: Sinha et al.* [63] *$\sum Q_{exc}$*

B. Elastic effects

From figure 4.20, the Q_{el} and Q_T data for molecule, C_3F_5N can be seen. Both the results are computed by employing two methods, viz., SCOP approach and 2p-SEM formalism. Across the entire energy range of 2p-SEM (i.e., 50-10000 eV), both results are seen to be overlapping with each other. No previous reported data available for Q_{el} and Q_T for the comparison.

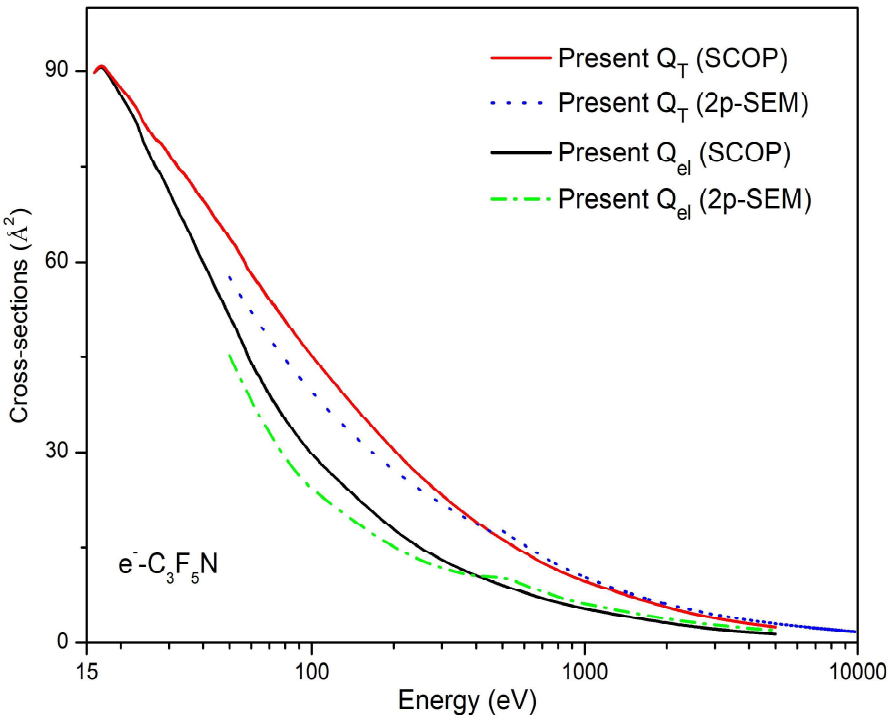

Figure 4.20 Elastic processes for C_3F_5N

Red solid: Present Q_T (SCOP); Dotted: Present Q_T (2p-SEM); Black dash: Present Q_{el} (SCOP); Cyan dash dot: Present Q_{el} (2p-SEM)

In the figure 4.21, the Q_{el} and Q_T data for molecule, C_4F_7N has been plotted. The results of Q_{el} and Q_T have been obtained from SCOP and 2p-SEM formalism. For this molecule also, the data of both the methodologies are seen to be in excellent agreement with each other. No previous reported data available for Q_{el} and Q_T for the comparison.

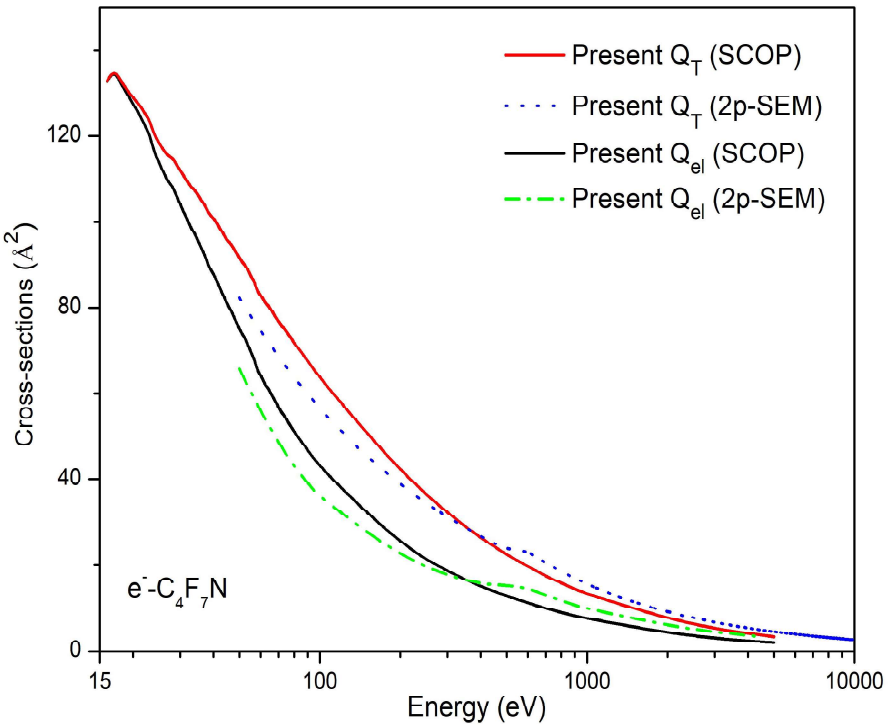

Figure 4.21 Elastic processes for C_4F_7N

Solid: Present Q_T (SCOP); Dotted: Present Q_T (2p-SEM); Dashed: Present Q_{el} (SCOP); Dash Dotted: Present Q_{el} (2p-SEM)

4.4 Correlations study

A. For Biomolecules

From the total electron scattering cross sections, Q_T obtained through 2p-SEM formalism, we have plotted various correlation graphs in figures 4.22 to 4.24 for molecules having 50-80 molecular electrons (i.e., DNA/RNA bases [66], Furfural and para-Benzoquinone).

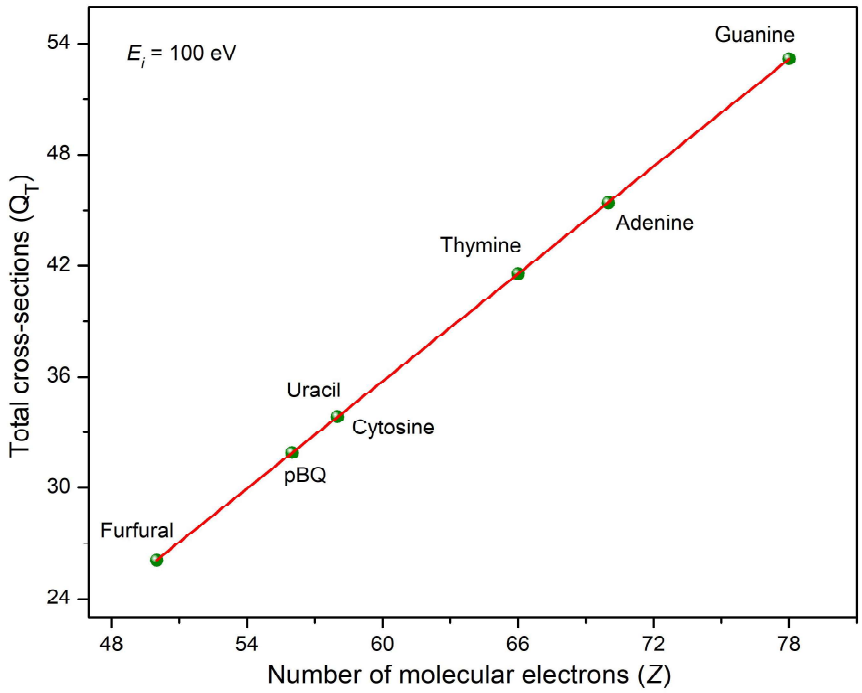

Figure 4.22 Correlation between Present Q_T (2p-SEM) and Z (Number of molecular electrons)

The correlation study is a very useful feature to determine the reliability and consistency of the cross sections data. The 2p-SEM method enables us to obtained reliable Q_T and Q_{el} for large and complex molecules $55 < Z < 95$ for a broad energy range 50 – 5000 eV. To check the self-consistency of the present data we have plotted various graphs between Q_T (2p-SEM) vs Z (number of target electrons) and Q_T vs N_v (number of valance electrons) in figure 4.22 and 4.23 at 100 eV, respectively. We observed the exact linear correlation between them, which reflects the size dependency of total cross-sections.

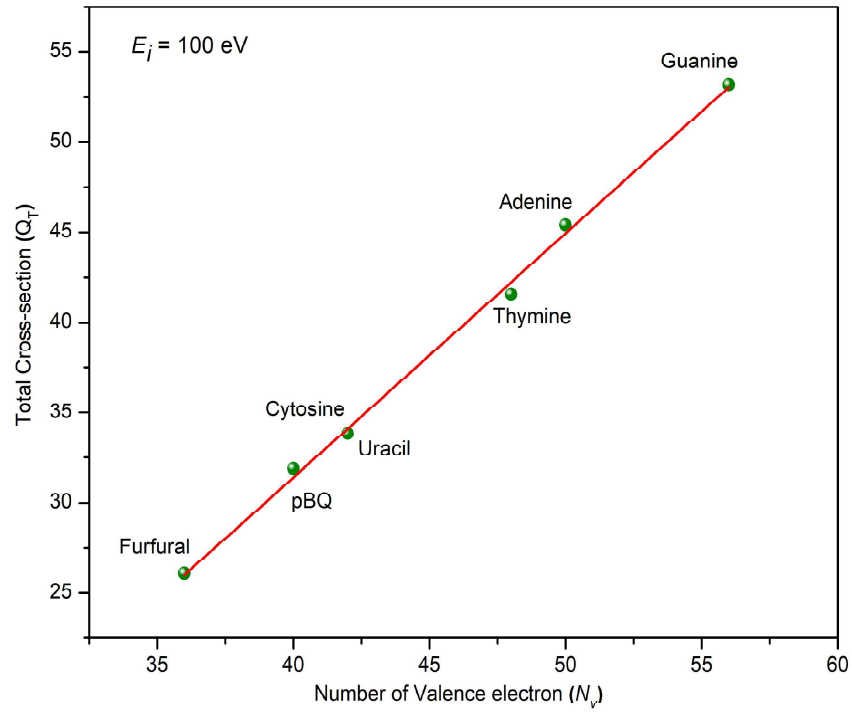

Figure 4.23 Correlation between Q_T (2p-SEM) and Number of valence electron (N_v)

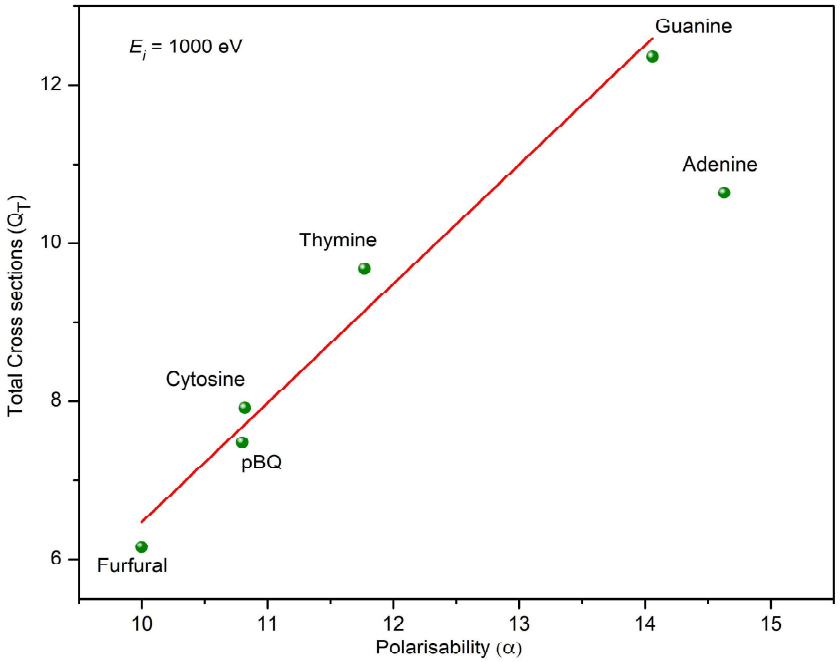

Figure 4.24 Correlation between Q_T and dipole polarizability (α)

Furthermore, the correlation of the molecular polarisability (α) with the Q_T and maximum ionisation cross-sections (Q_{ion}(peak)) are also examined. Figures 4.24 and 4.25 display the linear dependency of Q_T and Q_{ion}(peak) with molecular polarizability for the biocompounds ($50 < Z < 80$).

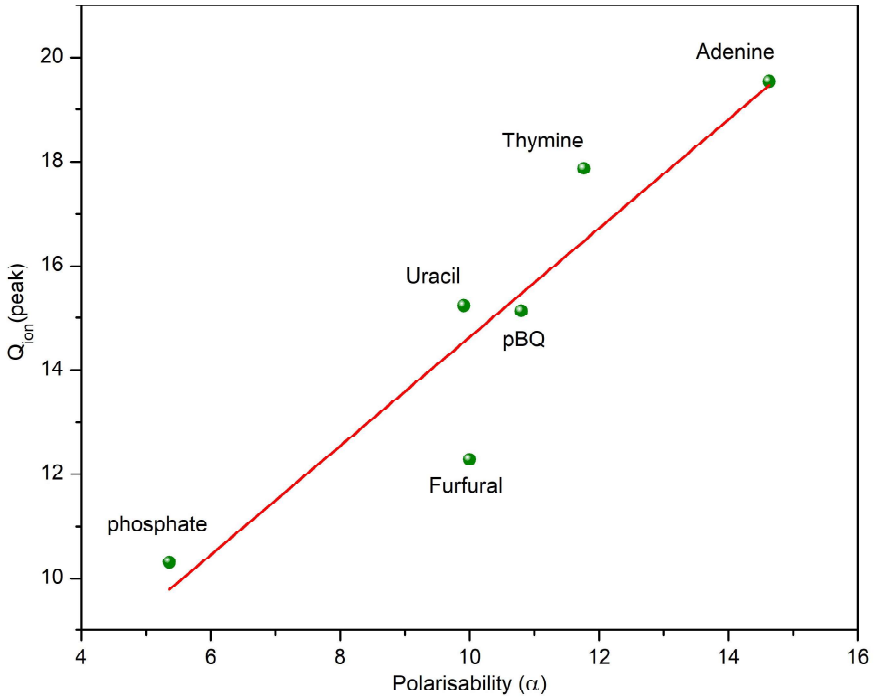

Figure 4.25 Correlation between Q_{ion}(peak) and dipole polarisability (α)

B. For fluorocompounds

The correlation study between the maximum Q_{ion} and various molecular properties, viz., size of the molecule in terms of the number of electrons (Z), molecular polarisability (α) and carbon atom number (N_c) involved in the molecule, has been conducted for C_3F_5N, C_4F_7N, and perfluoroketone (PFK) ($C_xF_{2x}O$, x=5-6) [67] molecules.

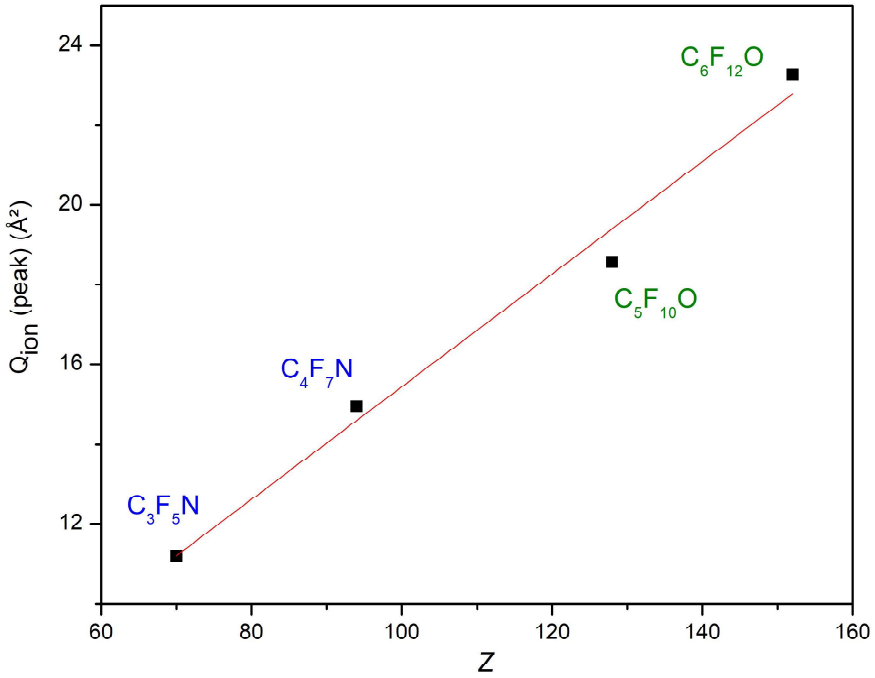

Figure 4.26 Correlation between Q_{ion} (peak) and Z

The linear relationship between the peak value of Q_{ion} and size of the molecules has been observed from the figure 4.26. The molecular charge cloud size (electron number, Z) has an important effect on the ionisation processes. The peak value of Q_{ion} rises swiftly as the charge cloud size become larger. However, along with size of the molecular charge cloud, Q_{ion} also depends on the molecular ionisation threshold, which is not greatly affected by the size of the molecules (table 4.6). As a result, Q_{ion} (peak) and Z are shown to have a linear connection (figure 4.26) through,

$$Q_{ion}(peak) = 0.1413\,Z + 1.3184$$

Table 4.6 Molecular properties and predicted α

Target	Z	Ionisation Energy (eV)	Polarizability ($10^{-24}cm^{-3}$)		
			Present	Estimated	Found at www.chemspider.com
C_3F_5N	70	15.20 [61]	5.72 [68]	5.97	
C_4F_7N	94	15.10 [61]	6.82 [68]	7.60	
$C_5F_{10}O$	128	12.02 [31]	8.83 [68]	9.84	10.6
$C_6F_{12}O$	152	11.41 [31]	11.44 [56]	12.54	12.6

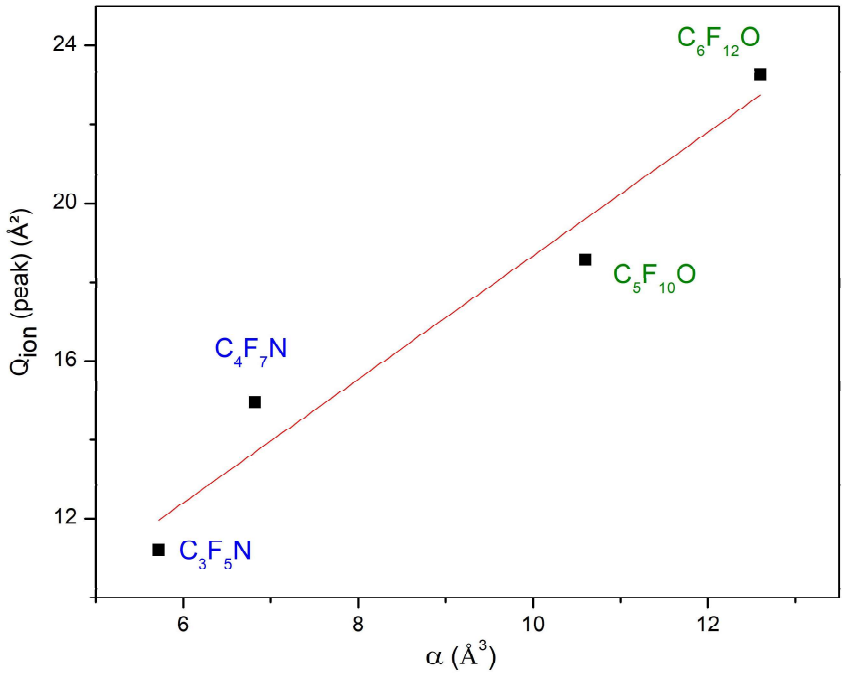

Figure 4.27 Correlation between Q_{ion} (peak) and polarizability (α)

In figure 4.27, we have plotted the peak value of Q_{ion} against the molecular polarisability (α) for fluoronitriles and fluoroketones and observed the liner relation between them as previously reported by Harland and Vallance [69] and Bart *et.al.* [70]. They both are linearly correlated with each other through the following equation,

$$Q_{ion}(peak) = 1.5668\,\alpha + 2.9996$$

This correlation between the Q_{ion} (peak) and molecular polarisability, allows us to predict one unknown parameter if the other is known. In table 4.6, the predicted polarisability has been tabulated with the existing one. An excellent matching between the predicted and available values of α, has been observed.

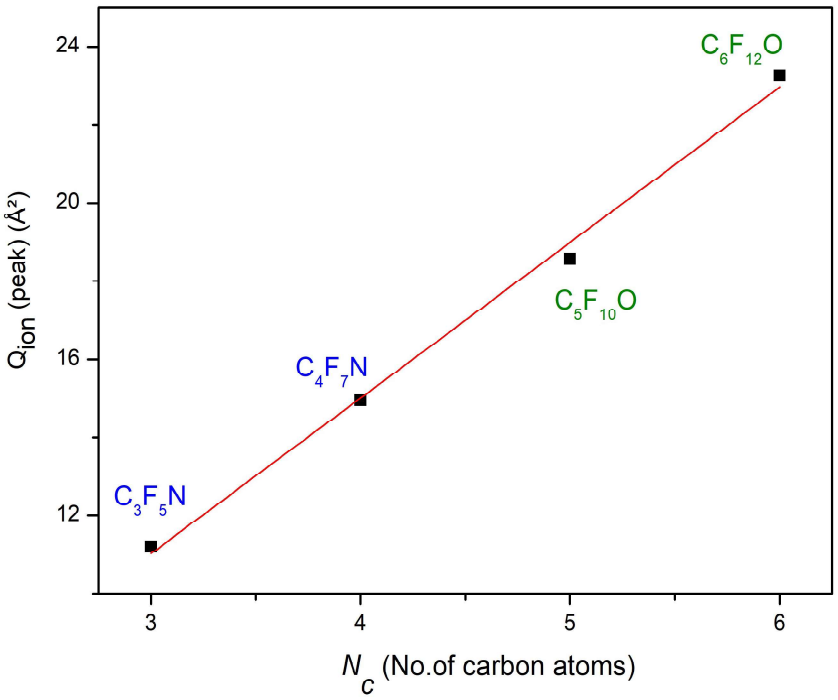

Figure 4.28 Variation of Q_{ion} (peak) with N_c

The similar linear trend has been observed between the Q_{ion} (peak) and N_c present in the fluoronitriles and fluoroketones. Figure 4.28 shows their liner relationship through,

$$Q_{ion}(peak) = 3.9842N_c - 0.9304$$

This linear relationship enables us to find out the Q_{ion} (peak) value for such a larger and complex molecule.

4.4.1 Computation of dielectric constant (ε)

The dielectric constant for para-Benzoquinone (pBQ) and furfural molecules has potential applications for the study of electrical energy storage device, pseudo capacitor, photo transistor, dye-sensitized solar cells, artificial photosynthesis, rechargeable batteries, the evolution of new electronic devices and other electrical properties.

The dielectric constant for fluoronitrile molecules has many applications for the study of electrical energy storage, the structure of high-performance electrical insulation materials, the evolution of new electronic devices and other electrical properties.

In the present work, we have estimated the dielectric constant value using Clausius-Mossotti, Onsager equation and from the correlation study of Q_{ion}(peak) and polarisability (α) as discussed in chapter II.

Table 4.7 Estimated dielectric constant (ε)

Target	N (molecules/cm^3)	α (Å^3)	ρ (g/cm^3)	M (g/mole)	Dielectric constant (ε)	
					CM equation [71]	Onsager equation [72]
$C_5H_4O_2$	7.27*10^{21}	10.00 [27]	1.16	96.10	2.31	0.99
$C_6H_4O_2$	7.35*10^{21}	10.80 [27]	1.32	108.10	2.49	1.00
C_3F_5N	5.45*10^{21}	5.72 [73]	1.76 [74]	195.03 [74]	1.44	0.96
C_4F_7N	4.67*10^{21}	6.82 [73]	1.70 [74]	219.05 [74]	1.46	1.07

We observed linear relationship between maximum ionisation cross section and dielectric constant from Clausius-Mossotti equation for biocompounds in figure 4.29 and for fluorocompounds in figure 4.30. Linear dependency of the Q_{ion} (peak) and dielectric constant can be observed for both biocompounds and fluorocompounds, which is expected from the linear dependency of the polarisabilty and ε from the Clausius-Massotti equation. This facilitates us to estimate the unknown parameter if other is known.

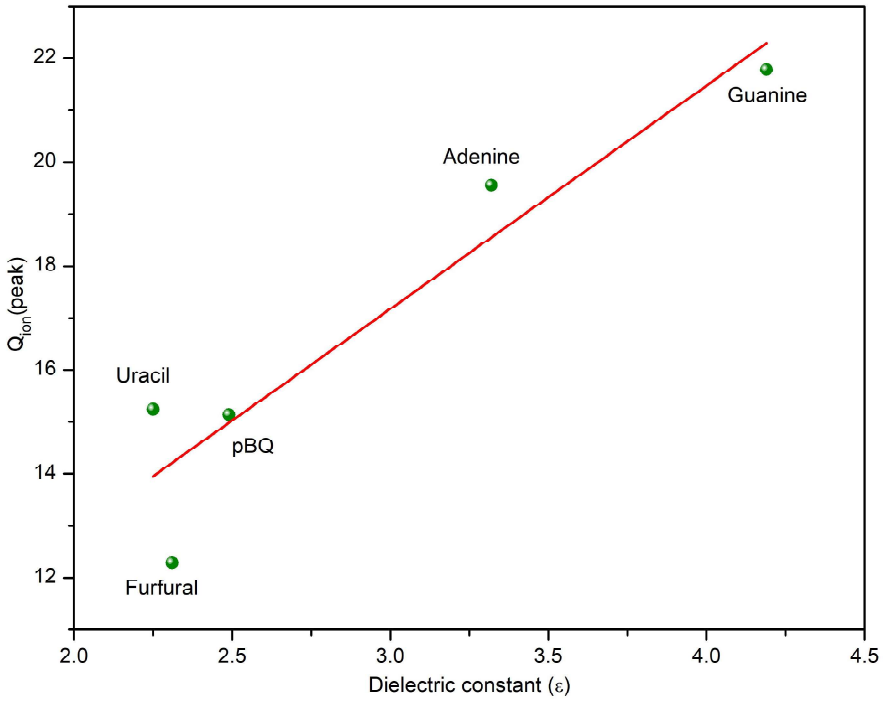

Figure 4.29 Correlation between Q_{ion}(peak) and dielecric constant (through CM equation)

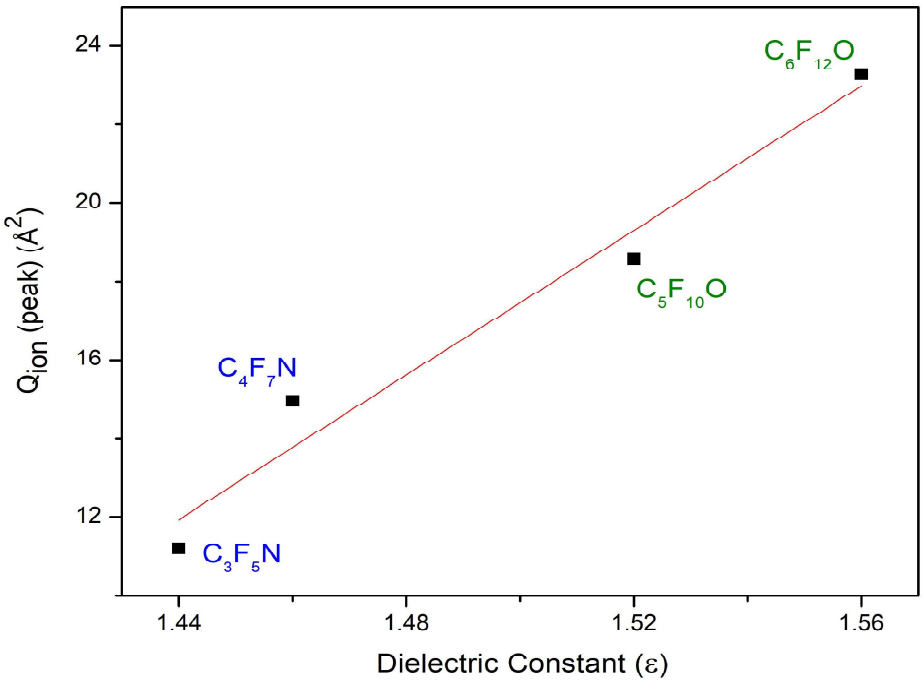

Figure 4.30 Variation of Q_{ion} (peak) with ε

Fluoronitriles, such as C_4F_7N and C_3F_5N, can have twice the dielectric strength of SF_6, as revealed by the experiment of J. C. Devins [74]. Comparing a composite material comprised of epoxy resin and C_3F_5N to pure epoxy resin, the electrical properties of the composite material revealed higher dielectric strength and thermal stability. An important factor in designing and optimising this composite material is the dielectric constant of C_3F_5N [75].

Also, due to its dielectric qualities, C_4F_7N has the potential to be used in power equipment as a high-performance insulating gas. Since C_4F_7N has a substantially higher dielectric constant than SF_6, a commonly used insulating gas, it may provide an intriguing replacement for usage in power equipment [50,51].

4.5 Bibliography

[1] D. Voet, and J. G. Voet, *Biochemistry*, second edition (John Wiley & Sons, New York, 1995).

[2] *Nucleosides*, https://en.wikipedia.org/wiki/Nucleoside#cite_note-2.

[3] D. C. Orr, H. T. Figueiredo, C. L. Mo, C. R. Penn, and J. M. Cameron, *DNA Chain Termination Activity and Inhibition of Human Immunodeficiency Virus Reverse Transcriptase by Carbocyclic 2',3'-Didehydro-2',3'-Dideoxyguanosine Triphosphate*, Journal of Biological Chemistry **267** (6), 4177-4182 (1992).

[4] G. Gumina, Y. Chong, H. Choo, G.-Y. Song, and C. Chu, *L - Nucleosides: Antiviral Activity and Molecular Mechanism*, Curr Top Med Chem **2**, 1065 (2002).

[5] G. Maga and S. Spadari, *Combinations Against Combinations: Associations of Anti-HIV 1 Reverse Transcriptase Drugs Challenged by Constellations of Drug Resistance Mutations*, Curr Drug Metab **3**, 73 (2002).

[6] K. S. Anderson, *Perspectives on the Molecular Mechanism of Inhibition and Toxicity of Nucleoside Analogs That Target HIV-1 Reverse Transcriptase*, Molecular Basis of Diseas **1587**, 296 (2002).

[7] M. A. Turner, X. Yang, D. Yin, K. Kuczera, R. T. Borchardt, and P. L. Howell, *Structure and Function of S-Adenosylhomocysteine Hydrolase*, Cell Biochem Biophys **33**, 101 (2000).

[8] J. de Vries, R. Hoekstra, R. Morgenstern, and T. Schlath lter, *C q -Induced Excitation and Fragmentation of Uracil: Effects of the Projectile Electronic Structure*, Journal of Physics B: Atomic, Molecular and Optical Physics **35**, 4373 (2002).

[9] L. Sanche, *Low Energy Electron-Driven Damage in Biomolecules*, European Physical Journal D **35**, 367 (2005).

[10] Y. Gao, Y. Zheng, and L. Sanche, *Low-Energy Electron Damage to Condensed-Phase DNA and Its Constituents*, Int J Mol Sci **22**, 7879 (2021).

[11] M. Vinodkumar and C. Limbachiya, *Electron Impact Total and Ionization Cross-Sections for DNA Based Compounds*, Mol Phys **111**, 215 (2013).

[12] M. Ashouri, M. Hajivaliei, and N. Gholami, *Dirac Partial Wave Calculation for Electron Scattering Cross Section by Nucleic Acid Bases*, Phys Scr **97**, 035402 (2022).

[13] M. A. Rehman and E. Krishnakumar, *Electron Impact Ionization of Adenine: Partial Cross Sections*, Atoms **10**, 100 (2022).

[14] Z. Deng, I. Bald, E. Illenberger, and M. A. Huels, *Beyond the Bragg Peak: Hyperthermal Heavy Ion Damage to DNA Components*, Phys Rev Lett **95**, 153201 (2005).

[15] M. A. H. Du Penhoat, P. López-Tarifa, K. K. Ghose, Y. Jeanvoine, M. P. Gaigeot, R. Vuilleumier, M. F. Politis, and M. C. Bacchus-Montabonel, *Modeling Proton-Induced Damage on 2-Deoxy-D-Ribose. Conformational Analysis*, J Mol Model **20**, (2014).

[16] Jun Ma, A. Kumar, Y. Muroya, S. Yamashita, T. Sakurai, S. A. Denisov, M. D. Sevilla, A. Adhikary, S. Seki, and M. Mostafavi, *Observation of Dissociative Quasi-Free Electron Attachment to Nucleoside via Excited Anion Radical in Solution*, Nat Commun **10**, 102 (2019).

[17] C. Winstead, and V. McKoy, *Resonant Interactions of Slow Electrons with DNA Constituents*, Radiation Physics and Chemistry **77**, 1258 (2008).

[18] C. Winstead, V. McKoy, and S. d'Almeida Sanchez, *Interaction of Low-Energy Electrons with the Pyrimidine Bases and Nucleosides of DNA*, J Chem Phys **127**, 085105 (2007).

[19] C. Winstead and V. McKoy, *Interaction of Low-Energy Electrons with the Purine Bases, Nucleosides, and Nucleotides of DNA*, J Chem Phys **125**, 244302 (2006).

[20] H. Nikjoo, S. Uehara, D. Emfietzoglou, and F. A. Cucinotta, *Track-Structure Codes in Radiation Research*, Radiat Meas **41**, 1052 (2006).

[21] D. Alloni, Scientifica Acta **1**, 164 (2007).

[22] M. Dingfelder, *Track-Structure Simulations for Charged Particles*, Health Phys **103**, 590 (2012).

[23] M. Vinodkumar, H. Bhutadia, C. Limbachiya, and K. N. Joshipura, *Electron Impact Total Ionization Cross Sections for H2S, PH3, HCHO and HCOOH*, Int J Mass Spectrom **308**, 35 (2011).

[24] M. Vinodkumar, C. Limbachiya, M. Barot, M. Swadia, and A. Barot, *Electron Impact Total Ionization Cross Sections for All the Components of DNA and RNA Molecule*, Int J Mass Spectrom **339–340**, 16 (2013).

[25] F. Blanco and G. García, *A Screening-Corrected Additivity Rule for the Calculation of Electron Scattering from Macro-Molecules*, Journal of Physics B: Atomic, Molecular and Optical Physics **42**, 145203 (2009).

[26] a) C. Yu, T. J. O'Donnell, and P. R. LeBreton, *Ultraviolet Photoelectron Studies of Volatile Nucleoside Models. Vertical Ionization Potential Measurements of Methylated Uridine, Thymidine, Cytidine, and Adenosine*, Journal of Physical Chemistry **85**, 3851 (1981).

b) Smruti Parikh, Chetan Limbachiya, *Electron driven molecular processes for Nucleosides*, Radiation Physics and Chemistry **208**, 110940 (2023).

[27] *ChemSpider*, http://www.chemspider.com/Default.aspx.

[28] P. Możejko, *Electron-Impact Ionization Cross Section Calculations for Selected Ribonucleosides*, J Phys Conf Ser **1412**, 152002 (2020).

[29] M. Vinodkumar, C. Limbachiya, H. Desai, and P. C. Vinodkumar, *Electron-Impact Total Cross Sections for Phosphorous Triflouride*, Phys Rev A (Coll Park) **89**, 062715 (2014).

[30] M. Vinodkumar, C. Limbachiya, A. Barot, and N. Mason, *Computation of Electron-Impact Rotationally Elastic Total Cross Sections for Methanol over an Extensive Range of Impact Energy (0.1 – 2000 EV)*, Phys Rev A (Coll Park) **87**, 012702 (2013).

[31] N. Thakkar, M. Swadia, M. Vinodkumar, N. Mason, and C. Limbachiya, *Electron Induced Elastic and Inelastic Processes for Perfluoroketone (PFK) Molecules*, Plasma Sources Sci Technol **30**, 085008 (2021).

[32] T. L. Junqueira, O. Cavalett, and A. Bonomi, *The Virtual Sugarcane Biorefinery—A Simulation Tool to Support Public Policies Formulation in Bioenergy* (Springer International Publishing, Switzerland, 2016).

[33] J. W. Tester, E. M. Drake, M. J. Driscoll, M. W. Golay, and W. A. Peters, *Sustainable Energy: Choosing Among Options*, 2nd editio (The MIT Press, Cambridge, MA, 2012).

[34] Jayr Amorim, Carlos Oliveira, Jorge A. Souza-Corrêa, and Macro A. Ridenti, *Treatment of Sugarcane Bagasse Lignin Employing Atmospheric Pressure Microplasma Jet in Argon*, Plasma Processes and Polymers **10**, (2013).

[35] Eliane M. de Oliveira, Sergio d'A. Sanchez, Márcio H. F. Bettega, Alexandra P. Natalense, Marco A. P. Lima, and Márcio T. do N. Varella, *Atomic and molecular collisions and interactions- Shape Resonance Spectra of Lignin Subunits*, Phys Rev A **86** (2), (2012).

[36] Eliane M. de Oliveira, Romarly F. da Costa, Sergio d'A. Sanchez, Alexandra P. P. Natalense, Márcio H. F. Bettega, Marco A. P. Lima, and Márcio T. do N. Varella, *Low-Energy Electron Scattering by Cellulose and Hemicellulose Components*, Physical Chemistry Chemical Physics **15**, (2013).

[37] Ajit Singh Mamman, Jong-Min Lee, Yeong-Cheol Kim, In Taek Hwang, No-Joong Park, Young Kyu Hwang, Jong-San Chang, Jin-Soo Hwang, *Furfural: Hemicellulose/Xylosederived Biochemical*, Biofuels, Bioproducts and Biorefining **2**, 438 (2008).

[38] K. J. Zeitsch, *The Chemistry and Technology of Furfural and Its ManyBy-Products*, 1st ed. (Elsevier science, 2000).

[39] H. Kobayashi and A. Fukuoka, *Synthesis and Utilisation of Sugar Compounds Derived from Lignocellulosic Biomass*, Green Chemistry **15**, 1740 (2013).

[40] A. W. Khan, J. P. Labrie, and J. McKeown, *Effect of Electron-Beam Irradiation Pretreatment on the Enzymatic Hydrolysis of Softwood*, Biotechnology Bioengineering **28**, (1986).

[41] Marco A. Ridenti, Jayr Amorim Filho, Michael J. Brunger, Romarly F. da Costa, Márcio T. do N. Varella, Márcio H.F. Bettega, and Marco A.P. Lima, *Electron Scattering by Biomass Molecular Fragments: Useful Data for Plasma Applications?*, The European Physical Journal D **70**, (2016).

[42] D. B. Jones, R. F. da Costa, M. T. D. N. Varella, M. H. F. Bettega, M. A. P. Lima, F. Blanco, G. García, and M. J. Brunger, *Integral Elastic, Electronic-State, Ionization, and Total Cross Sections for Electron Scattering with Furfural*, Journal of Chemical Physics **144**, (2016).

[43] W. S. & P. O. Athina Zouni, Horst-Tobias Witt, Jan Kern, Petra Fromme, Norbert Krauss, *Crystal Structure of Photosystem II from Synechococcus Elongatus at 3.8 Å Resolution*, Nature **409**, 739 (2001).

[44] M. Hambourger, G. F. Moore, D. M. Kramer, D. Gust, A. L. Moore, and T. A. Moore, *Biology and Technology for Photochemical Fuel Production*, Chemical Society Review **38**, 25 (2009).

[45] O. Yehezkeli, R. Tel-Vered, J. Wasserman, A. Trifonov, D. Michaeli, R. Nechushtai, and I. Willner, *Integrated Photosystem II-Based Photo-Bioelectrochemical Cells*, Nat Commun **3**, 742 (2012).

[46] A. Traoré Dubuis, A. Verkhovtsev, L. Ellis-Gibbings, K. Krupa, F. Blanco, D. B. Jones, M. J. Brunger, and G. García, *Total Cross Section of Furfural by Electron Impact: Experiment and Theory*, Journal of Chemical Physics **147**, (2017).

[47] A. I. Lozano, K. Krupa, F. Ferreira da Silva, P. Limão-Vieira, F. Blanco, A. Muñoz, D. B. Jones, M. J. Brunger, and G. García, *Low Energy Electron Transport in Furfural*, European Physical Journal D **71**, (2017).

[48] A. I. Lozano et al., *Total Electron Scattering Cross Sections from Para -Benzoquinone in the Energy Range 1-200 eV*, Physical Chemistry Chemical Physics **20**, 22368 (2018).

[49] D. B. Jones, R. F. da Costa, F. Kossoski, M. T. D. N. Varella, M. H. F. Bettega, G. García, F. Blanco, R. D. White, M. A. P. Lima, and M. J. Brunger, *Integral Elastic, Vibrational-Excitation, Electronic-State Excitation, Ionization, and Total Cross Sections for Electron Scattering from Para -Benzoquinone*, Journal of Chemical Physics **148**, (2018).

[50] Y. K. Kim and M. E. Rudd, *Binary-Encounter-Dipole Model for Electron-Impact Ionization*, Phys Rev A (Coll Park) **50**, 3954 (1994).

[51] G. García and F. Maneró, *Correlation of the Total Cross Section for Electron Scattering by Molecules with 10-22 Electrons, and Some Molecular Parameters at Intermediate Energies*, Chem Phys Lett **280**, 419 (1997).

[52] X. Li, H. Zhao, and A. B. Murphy, *SF6-Alternative Gases for Application in Gas-Insulated Switchgear*, J Phys D Appl Phys **51**, (2018).

[53] Xiaoxing Zhang, Yi Li, Song Xiao, Ju Tang, Shuangshuang Tian, and Zaitao Deng *Decomposition Mechanism of C5F10O: An Environmentally Friendly Insulation Medium*, Environ Sci Technol **51**, 10127 (2017).

[54] J. D. Mantilla, N. Gariboldi, S. Grob, and M. Claessens, *Investigation of the Insulation Performance of a New Gas Mixture with Extremely Low GWP*, in *2014 IEEE Electrical Insulation Conference (EIC)* (IEEE, Philadelphia, PA, USA, 2014), pp. 469–473.

[55] J. D. Mantilla, N. Gariboldi, S. Grob, and M. Claessens, *Investigation of the Insulation Performance of a New Gas Mixture with Extremely Low GWP*, EIC 2014 - Proceedings of the 32nd Electrical Insulation Conference 469 (2014).

[56] X. Yu, H. Hou, and B. Wang, *Prediction on Dielectric Strength and Boiling Point of Gaseous Molecules for Replacement of SF6*, J Comput Chem **38**, 721 (2017).

[57] Y. K. Deng and D. M. Xiao, *The Effective Ionization Coefficients and Electron Drift Velocities in Gas Mixtures of CF3I with N2 and CO2 Obtained from Boltzmann Equation Analysis*, Chinese Physics B **22**, (2013).

[58] Y. K. Kim, W. Hwang, N. M. Weinberger, M. A. Ali, and M. E. Rudd, *Electron-Impact Ionization Cross Sections of Atmospheric Molecules*, Journal of Chemical Physics **106**, 1026 (1997).

[59] J. Xiong, X. Li, J. Wu, X. Guo, and H. Zhao, *Calculations of Total Electron-Impact Ionization Cross Sections for Fluoroketone C5F10O and Fluoronitrile C4F7N Using Modified Deutsch-Märk Formula*, J Phys D Appl Phys **50**, 2 (2017).

[60] C. Limbachiya, M. Vinodkumar, M. Swadia, K. N. Joshipura, and N. Mason, *Electron-Impact Total Cross Sections for Inelastic Processes for Furan, Tetrahydrofuran and 2,5-Dimethylfuran*, Mol Phys **113**, 55 (2015).

[61] F. Wang, Q. Dun, S. Chen, L. Zhong, X. Fan, and L. L. Li, *Calculations of Total Electron Impact Ionization Cross Sections for Fluoroketone and Fluoronitrile*, IEEE Transactions on Dielectrics and Electrical Insulation **26**, 1693 (2019).

[62] M. Ranković, J. Chalabala, M. Zawadzki, J. Kočišek, P. Slavíček, and J. Fedor, *Dissociative Ionization Dynamics of Dielectric Gas C3F7CN*, Physical Chemistry Chemical Physics **21**, 16451 (2019).

[63] N. Sinha, V. M. Patel, and B. Antony, *Ionization Cross Sections for Plasma Relevant Molecules*, Journal of Physics B: Atomic, Molecular and Optical Physics **53**, (2020).

[64] Y.-K. Kim and P. M. Stone, *Ionization of Boron, Aluminum, Gallium, and Indium by Electron Impact*, Phys Rev A **64**, 052707 (2001).

[65] Chetan Limbachiya, Minaxi Vinodkumar, Mohit Swadia and Avani Barot, *Electron Impact Total Cross Section Calculations for CH3SH (Methanethiol) from Threshold to 5 KeV*, Mol Phys **112**, 101 (2014).

[66] M. Vinodkumar, C. Limbachiya, M. Barot, A. Barot, and M. Swadia, *Electron Impact Total Cross Sections for Components of DNA and RNA Molecules*, Int J Mass Spectrom **360**, 1 (2014).

[67] N. Thakkar, M. Swadia, M. Vinodkumar, N. Mason, and C. Limbachiya, *Electron Induced Elastic and Inelastic Processes for Perfluoroketone (PFK) Molecules*, Plasma Sources Sci Technol **30**, (2021).

[68] N. Sinha, V. M. Patel, and B. Antony, *Ionization Cross Sections for Plasma Relevant Molecules*, Journal of Physics B: Atomic, Molecular and Optical Physics **53**, 145101 (2020).

[69] P. W. Harland and C. Vallance, *Ionization Cross-Sections and Ionization Efficiency Curves from Polarizability Volumes and Ionization Potentials*, Int J Mass Spectrom Ion Process **171**, 173 (1997).

[70] J. N. Bull, P. W. Harland, and C. Vallance, *Absolute Total Electron Impact Ionization Cross-Sections for Many-Atom Organic and Halocarbon Species*, Journal of Physical Chemistry A **116**, 767 (2012).

[71] C. Kittel and D. F. Holcomb, *Introduction to Solid State Physics*, 8th ed., Vol. 35 (1967).

[72] L. Onsager, *Electric Moments of Molecules in Liquids*, J Am Chem Soc **58**, 1486 (1936).

[73] Y. Wu, C. Wang, H. Sun, A. B. Murphy, M. Rong, F. Yang, Z. Chen, C. Niu, and X. Wang, *Properties of C4F7N-CO2 Thermal Plasmas: Thermodynamic Properties, Transport Coefficients and Emission Coefficients*, J Phys D Appl Phys **51**, (2018).

[74] D. P, *CRC Handbook of Chemistry and Physics*, Vol. 268 (CRC Press, 1992).

[75] J. Jiao, D. Xiao, X. Zhao, and Y. Deng, *Analysis of the Molecules Structure and Vertical Electron Affinity of Organic Gas Impact on Electric Strength*, Plasma Science and Technology **18**, 554 (2016).

[76] R. E. Wootton et al., Gases Superior To Sf6 for Insulation and Interruption., 1982.

[77] R. Qiu, W. Zhou, Y. Zheng, S. Hu, H. Li, and J. Yu, *A Simulation Research on Diffusion Processes of Discharging Decomposition Products of C4F7N/CO2 in Gas Insulated*

Transmission Lines, 7th IEEE International Conference on High Voltage Engineering and Application, ICHVE 2020 - Proceedings 20 (2020).

[78] N. Tang, L. Chen, B. Zhang, and X. Li, *Experimental and Theoretical Exploration of C4F7N Gas Decomposition under Partial Discharge*, 7th IEEE International Conference on High Voltage Engineering and Application, ICHVE 2020 - Proceedings 4 (2020).